10 min for antigen retrieval. Immunohistochemical staining was then performed with rabbit polyclonal anti-OCIAD2 antibody diluted 1:1000 (Takara Bio, Shiga, Japan) using a HISTOSTAINER 36A autostainer (Nichirei, Tokyo, Japan). Using the same sections, immunohistochemical staining was also performed with a mouse monoclonal anti-CEA (carcinoembryonic antigen, clone CEM010) antibody diluted 1:200 (Takara Bio), without antigen retrieval treatment, and with a rabbit polyclonal anti-OCIAD1 antibody diluted 1:400 (Proteintech Group Inc, Chicago, IL, USA) with antigen retrieval using TE buffer at 105°C for 15 min.

Evaluation of immunoreactivity and statistical analysis

For evaluation of OCIAD2 and OCIAD1 staining, we used a case of lung adenocarcinoma as a positive control. This case had been confirmed to show high expression of OCIAD2 by RT-PCR and *in situ* hybridization (data not shown). The cytoplasmic granular staining pattern of the tumor cells was judged to be positive. For evaluation of CEA staining, we used a case of colonic adenocarcinoma as a positive control. This case revealed a significantly higher serum CEA level (20 ng/ml) and showed a diffuse cytoplasmic staining pattern (not apical staining showing polarity) that was judged as positive.

As all of the benign adenomas showed less than 30% staining for CEA per case, we defined positivity in 30% or more of the tumor area as positive. The intensity of staining with each antibody in positive cases was easily judged, and we did not use the staining intensity as a positive criterion. To examine the association between OCIAD2, OICIAD1, CEA and tumor malignancy, we used the χ^2 test. To evaluate the correlation between OCIAD2, OCIAD1 and CEA positivity, we used Spearman's rank correlation test.

RESULTS

Immunohistochemical staining of OCIAD2, OCIAD1 and CEA

OCIAD2 was detected in the cytoplasm of the tumor cells of ovarian mucinous tumor. They showed a granular staining pattern, similar to the cases of lung adenocarcinoma that were positive for OCIAD2. Unlike lung cancer, however, secreted mucin was stained as background.

Among the 43 cases of mucinous adenoma, 6 (14%) showed positive staining for OCIAD2 (Table 2, Fig. 2a). In the tumor cell cytoplasm, OCIAD2 showed a granular staining pattern that was separated from intracytoplasmic mucin. Secreted mucin was also stained in intracystic areas and the brush border. Sometimes, nuclei of tumor cells were also stained, but this staining was judged as negative. Among the 40 cases of mucinous borderline tumor, 25 (63%) including 8 of 10 of the endocervical type (80%) showed positive staining for OCIAD2 (Table 2, Fig. 2b, c). There was also background positive staining for secreted mucin in intracystic areas and the brush border. The nuclei of tumor cells showed nonspecific staining, but this was judged as negative. The cytoplasm of the tumor cells showed a granular OCIAD2 staining pattern like that of adenoma, and also positive staining for mucin when mucin secretion was abundant. Areas of papillary proliferation showed strongly positive staining for OCIAD2 in comparison to flat lining tumor cells (Fig. 3a). Among the 34 cases of mucinous carcinoma, 26 (74%) (6 of the infiltrating invasive type and 20 of the expansile invasive type) showed positive staining for OCIAD2 (Table 2, Fig. 2d). Areas of stromal invasion showed strongly positive staining for OCIAD2 in comparison with flat lining tumor cells (Fig. 3b).

The stainability of OCIAD1 was similar to that of OCIAD2, and positive staining for secreted mucin at the brush border was also evident. However, staining for intracystic secreted mucin and staining of nuclei were unremarkable. Among the 43 cases of mucinous adenoma, 21 (49%) were positive for OCIAD1 (Table 2, Fig. 4a). In the tumor cell cytoplasm, OCIAD1 showed a granular staining pattern that was separated from intracytoplasmic mucin like that of OCIAD2. On the other hand, unlike OCIAD2, positive staining was evident in the stromal cells. Among the 40 cases of mucinous borderline tumor, 26 (65%) including 9 among 10 of the endocervical type (90%) were positive for OCIAD1 (Table 2, Fig. 4b, c). Similarly to adenoma, OCIAD1 showed a granular staining pattern in the cytoplasm of the tumor cells. The tumor stroma also showed staining in the stromal cells. Several cases showed positive staining only in the stromal cells, whereas the tumor cells were negative. Among the 34 cases of mucinous carcinoma, 30 (86%) (7 of the infiltrating invasive type and 23 of the expansile invasive type) were positive

Table 2 Immunohistochemical results of OCIAD2, OCIAD1 and CEA

	N		OCIAD2		OCIAD1		CEA	
Mucinous adenoma	43		6 (14)		21 (49)		0 (0)	
Mucinous borderline tumor	Endocervical 10	40	8 (80)	25 (63)	9 (90)	26 (65)	5 (50)	10 (25)
	Intestinal 30		17 (57)		17 (57)		5 (17)	
Mucinous adenocarcinoma	Infiltrating 8	34	6 (75)	26 (76)	7 (88)	30 (88)	5 (63)	25 (74)
	Expansile 26		20 (77)		23 (88)		20 (77)	
Total	117		57 (49)		77 (66)		35 (30)	

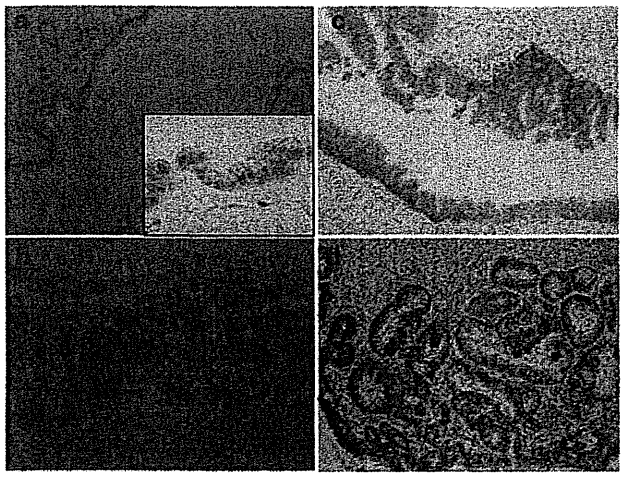

Figure 2 Immuohistocheical staining of ovarian cancer immunoreactive antigen domain containing 2 (OCIAD2) in mucinous ovarian tumors. Immunohistochemistry of OCIAD2 for adenoma (2a), borderline lesion (endocervical type) (2b), borderline lesion (intestinal type) (2c), and adenocarcinoma (2d). OCIAD2 is granularly positive in borderline tumor and carcinoma.

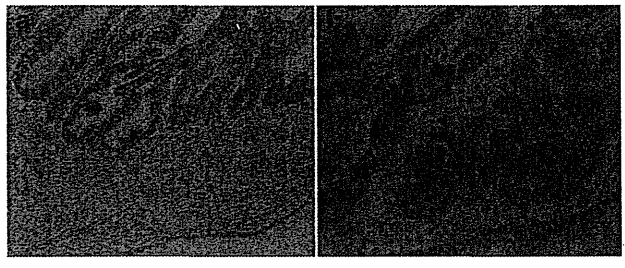

Figure 3 Histological staining pattern of ovarian cancer immunoreactive antigen domain containing 2 (OCIAD2) for OCIAD2 in mucinous borderline tumors and invasing mucinous adenocarcinoma. (a) Immunohistochemial staining of OCIAD2 for the case of mucinous borderline tumor. Areas of papillary proliferation showed more intense reactivity for OCIAD2 than flat lining tumor cells. (b) Immunohistochemical staining of OCIAD2 in a case of mucinous adenocarcinoma. Areas of stromal invasion (arrow heads) showed more intense reactivity for OCIAD 2 than flat lining tumor cells.

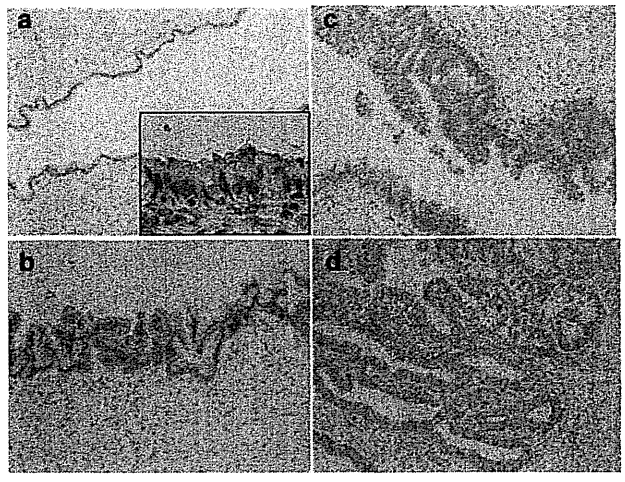

Figure 4 Immuohistocheical staining of ovarian cancer immunoreactive antigen domain containing 1 (OCIAD1) in mucinous ovarian tumors. Immunohistochemistry of OCIAD1 for adenoma (4a), borderline lesion (endocervical type) (4b), borderline lesion (intestinal type) (4c), and adenocarcinoma (4d). OCIAD1 is granularly positive in borderline tumor and carcinoma.

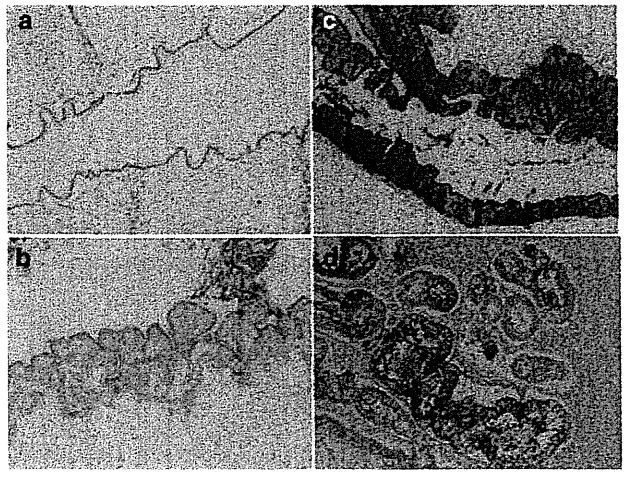

Figure 5 Immuohistocheical staining of CEA in mucinous ovarian tumors. Immunohistochemistry of CEA for adenoma (5a), borderline lesion (endocervical type) (5b), borderline lesion (intestinal type) (5c), and adenocarcinoma (5d). CEA is granularly positive in borderline tumor and carcinoma.

for OCIAD1 (Table 2, Fig. 4d). As was the case in adenocarcinoma, OCIAD1 showed a granular staining pattern that was separated from intracytoplasmic mucin. Stromal cells also showed positive background staining.

With regard to CEA, tumor cells showed a diffuse cytoplasmic staining pattern, as had been observed in colonic adenocarcinoma, and also positive staining for mucin. Among the 43 cases of mucinous adenoma, 0 (0%) were positive for CEA (Table 2, Fig. 5a). Background staining for intracystic and brush border secreted mucin was evident, but this was judged as negative. Among the 40 cases of mucinous borderline tumor, 10 (25%) including five among ten of the endocervical type (50%) were positive for CEA (Table 2, Fig. 5b, c). There was strongly positive background staining for intracystic and brush border secreted mucin. Non-specific positive staining was evident in the nuclei of tumor cells and in the tumor stroma. Among the 34 cases of mucinous carcinoma, 25 (71%) (5 of the infiltrating invasive type and 20 of the expansile invasive type) were positive for CEA (Table 2, Fig. 5d). Strongly positive background staining for intracystic and brush border secreted mucin was evident, similarly to adenoma and borderline lesions. Diffuse cytoplasmic staining was judged as positive. The tumor cell nucleoli and tumor stroma showed non-specific positive staining.

The one case of borderline tumor showing pseudomyxoma peritonei was stained with OCIAD2, but negative for OCIAD1 and CEA.

Statistical analysis

Positivity for OCIAD2 increased gradually with tumor progression, and more than 70% of the mucinous carcinomas were positive (Table 2). A similar tendency was seen for CEA and OCIAD1, more than 70% of the carcinomas also being positive. The expression of OCIAD2, CEA and OCIAD1 increased significantly as the malignancy of the tumor increased ($P < 0.01$, $P < 0.01$, and $P < 0.01$, respectively). Table 2 compares the positivity ratio of adenoma vs borderline lesion and adenocarcinoma. Among the cases of adenoma, 6 (14%), 21 (49%), and 0 (0%) were positive for OCIAD2, OCIAD1, and CEA, respectively, whereas among the cases of borderline lesion and adenocarcinoma, 51 (68%), 56 (75%), and 35 (47%) were positive, respectively.

DISCUSSION

The ovarian cancer immunoreactive antigen domain (OCIAD) family comprises OCIAD1 and OCIAD2. In 2001, Luo *et al.* immunoscreened an ovarian carcinoma cDNA expression library using ascites from a patient with ovarian cancer and detected an antibody against OCIAD1.[8] Therefore, OCIAD1 is thought to be a cancer-specific protein that could be applicable for detection of carcinoma, and several reports have stressed the association between ovarian carcinoma malignancy and OCIAD1 expression. On the other hand, OCIAD2 was identified in 2001 by Strausberg *et al.* on the basis of its sequence similarity to OCIAD1 through the National Institute of Health Mammalian Gene Collection project.[19] Although OCIAD2 has high homology with OCIAD1, to date, no reports have examined the relationship between its expression and carcinoma or autoantibody against human tissue. Ishiyama T. first reported the association between lung adenocarcinogenesis and OCIAD2 on the basis of a cDNA microarray study.[7] In the present study, we examined the expression of OCIAD2 in ovarian carcinoma, especially ovarian mucinous tumors, since the diagnosis of their malignancy is based on histology, and no biomarkers for these tumors have been characterized.

In order to examine the relationship between the OCIAD family and other immunohistochemical biomarkers, we also examined the expression of CEA. As Table 2 shows, OCIAD2 expression was detected in 74% of mucinous ovarian carcinomas and 63% of borderline tumors (i.e. 69% of ovarian mucinous tumors with malignancy), but in only 14% of mucinous adenomas (benign counterpart) ($P < 0.01$). Expression of OCIAD2 was associated with the malignancy of ovarian mucinous tumors. OCIAD2 showed a granular staining pattern in the cytoplasm of the tumor cells, but interestingly its positivity was stronger in areas of papillary proliferation and stromal invasion than in flat tumor cells, suggesting an association between OCIAD2 expression and tumor malignancy.

With regard to borderline tumors, it was of considerable interest that positivity for all of the markers examined (OCIAD2, OCIAD1, and CEA) had a tendency to be higher in the endocervical type than in the intestinal type. As the tumor cells of intestinal-type tumors contain much mucin in their cytoplasim, relative to those of endocervical-type tumors, it might be difficult to judge the staining positivity of intestinal-type tumors. On the other hand, in the carcinomas, the rates of positivity for the three proteins showed no significant difference between the infiltrating invasive type and the expansile invasive type.

The staining patterns of OCIAD1 and CEA were similar to that of OCIAD2, but several differences were evident. OCIAD1 was positive in 86% of carcinomas and 65% of borderline tumors (i.e. 75% of all ovarian mucinous tumors with malignancy), whereas 49% of adenomas were also positive for OCIAD1. These results indicated that positivity for OCIAD1 increased in the earlier stage of malignant progression. Although we are unable to verify whether the staining was non-specific, stromal cells also showed positive staining for OCIAD1. However, the results suggested that OCIAD2 is a marker more associated with malignancy of ovarian mucinous tumor cells than is OCIAD1.

CEA was immunopositive in 71% of carcinomas and 25% of borderline tumors (i.e. 47% of all ovarian mucinous tumors with malignancy). The specificity of CEA for diagnosis of malignancy in ovarian mucinous tumors was highest among the three markers we examined, thus confirming that CEA is a very useful biomarker for detection of ovarian tumors. The CEA positivity rate mainly increased during the course from borderline tumor to carcinoma. Therefore, CEA might be a marker of more advanced-stage mucinous tumors in comparison with OCIAD2.

The association between OCIAD2 stainability and tumor malignancy was of considerable interest; papillary proliferating and invasive tumor cells were positive, whereas flat lining tumor cells were negative. Six cases of adenoma gave a positive reaction with anti-OCIAD2 antibody. These tumors were histologically diagnosed as adenoma, but may have had the potential to progress to borderline tumors. As it has been suggested that OCIAD2 may be localized to the tumor cell membrane, OCIAD2 protein in exfoliated tumor cells or cell fragments in ascites or blood could be detectable and applicable as a new biomarker of ovarian mucinous tumors.

In summary, we have demonstrated specific expression of OCIAD2 in ovarian mucinous tumors. Immunohistochemi-

cally. OCIAD2 appeared to be more specific than OCIAD1 and more sensitive than CEA. Examination of OCIAD2 expression is thus expected to become a new immunohistochemical biomarker of the malignancy of ovarian mucinous tumors. OCIAD2 is a membrane-localized protein expressed in several malignant tumors including lung cancer and ovarian cancers, but its function is still unclear. As normal tissue is unreactive with a specific antibody against OCIAD2, it appears that OCIAD2 is not a basic protein required for the survival of human cells. However, the biological implications of OCIAD2 should be examined extensively and utilized for the detection or treatment of malignant tumors expressing it.

REFERENCES

1 Feeley KM, Wells M. Precursor lesions of ovarian epithelial malignancy. *Histopathol* 2001; **38**: 87–95.
2 Shih IEM, Kurman RJ. Ovarian Tumorigenesis: A Proposed Model Based on Morphological and Molecular Genetic Analysis. *Am J Pathol* 2004; **164**: 1511–8.
3 Kurman RJ, Shih IEM. Molecular pathogenesis and extraovarian origin of epithelial ovarian cancer-shifting the paradigm. *Hum Pathol* 2011; **42**: 918–31.
4 Auner V, Kriegshäuser G, Tong D *et al.* KRAS mutation analysis in ovarian samples using a high sensitivity biochip assay. *BMC Cancer* 2009; **9**: 111–8.
5 Kurman RJ, Visvanathan K, Roden R *et al.* Early detection and treatment of ovarian cancer: Shifting from early stage to minimal volume of disease based on a new model of carcinogenesis. *Am J Obstet Gynecol* 2008; **198**: 351–6.
6 Kurman RJ, Shil IEM. Pathogenesis of Ovarian Cancer. Lessons from Morphology and Molecular Biology and their Clinical Implications. *Int J Gynecol Pathol* 2008; **27**: 151–60.
7 Ishiyama T, Kano J, Anami Y *et al.* OCIA domain containing 2 is highly expressed in adenocarcinoma mixed subtype with bronchioloalveolar carcinoma component and is associated with better prognosis. *Cancer Sci* 2007; **98**: 50–7.
8 Luo LY, Soosaipillai A, Diamandis EP. Molecular cloning of a novel human gene on chromosome 4p11 by immunoscreening of an ovarian carcinoma cDNA library. *Biochem Biophys Res Commun* 2001; **280**: 401–6.
9 Sengupta S, Michener CM, Escober P *et al.* Ovarian cancer immuno-reactive antigen domain containimg 1 (OCIAD1), a key player in ovarian cancer cell adhesion. *Gynecol Oncol* 2008; **109**: 226–33.
10 Wang C, Michener CM, Belinson JL *et al.* Role of the 18:1 lysophosphatidic acid-ovarian cancer immunoreactive antigen domain containing 1 (OCIAD1)-integrin axis in generating late-stage ovarian cancer. *Mol Cancer Ther* 2010; **9**: 1709–18.
11 Tavassoli FA, Devilee P, eds. *World Health Organization: Tumours of the Breast and Female Genital Organs (WHO/IARC Classification of Tumours)*. Lyon: IARC Press, 2003.
12 Cho KR, Shih IEM. Ovarian cancer. *Annu Rev Pathol* 2009; **4**: 287–313.
13 Kaku T, Ogawa S, Kawano Y *et al.* Histological classification of ovarian cancer. *Med Electron Microsc* 2003; **36**: 9–17.
14 Koskas M, Uzan C, Gouy S *et al.* Prognostic factors of a large retrospective series of mucinous borderline tumors of the ovary (excluding peritoneal pseudomyxoma). *Ann Surg Oncol* 2011; **18**: 40–8.
15 McCluggage WG. The pathology of and controversial aspects of ovarian borderline tumors. *Curr Opin Oncol* 2010; **22**: 462–72.
16 Hart WR. Borderline epithelial tumors of the ovary. *Mod Pathol* 2005; **18**: 33–50.
17 Chen S, Leitao MM, Tornos C *et al.* Invasion patterns in stage I endometrioid and mucinous ovarian carcinomas: A clinicopathologic analysis emphasizing favorable outcomes in carcinomas without destructive stromal invasion and the occasional malignant course of carcinomas with limited destructive stromal invasion. *Mod Pathol* 2005; **18**: 903–11.
18 Nomura K, Aizawa S. Noninvasive, microinvasive, and invasive mucinous carcinomas of the ovary: A clinicopathologic analysis of 40 cases. *Cancer* 2000; **89**: 1541–6.
19 Strausberg RL, Feingold EA, Grouse LH *et al.* Generation and initial analysis of more than 15,000 full-length human and mouse CDNA sequences. *Proc Natl Acad Sci USA* 2002; **99**: 16899–903.

International Journal of Gynecological Pathology
32:26–30, Lippincott Williams & Wilkins, Baltimore

Original Article

The Origin of Stroma Surrounding Epithelial Ovarian Cancer Cells

Tomoko Akahane, Akira Hirasawa, M.D., Ph.D., Hiroshi Tsuda, M.D., Ph.D., Fumio Kataoka, M.D., Sadako Nishimura, M.D., Ph.D., Hideo Tanaka, Eiichiro Tominaga, M.D., Ph.D., Hiroyuki Nomura, M.D., Ph.D., Tatsuyuki Chiyoda, M.D., Yoko Iguchi, M.D., Wataru Yamagami, M.D., Ph.D., Nobuyuki Susumu, M.D., Ph.D., and Daisuke Aoki, M.D., Ph.D.

Summary: Cancer stroma is thought to play an important role in tumor behavior, including invasion or metastasis and response to therapy. Cancer stroma is generally thought either to be non-neoplastic cells, including tissue-marrow or bone-marrow-derived fibroblasts, or to originate in epithelial mesenchymal transition of cancer cells. In this study, we evaluated the status of the *p53* gene in both the cancer cells and the cancer stroma in epithelial ovarian cancer (EOC) to elucidate the origin of the stroma. Samples from 16 EOC patients were included in this study. Tumor cells and adjacent nontumor stromal cells were microdissected and DNA was extracted separately. We analyzed *p53* sequences (exons 5–8) of both cancer and stromal tissues in all cases. Furthermore, we examined p53 protein expression in all cases. Mutations in *p53* were detected in 9 of the 16 EOCs: in 8 of these cases, the mutations were detected only in cancer cells. In 1 case, the same mutation (R248Q) was detected in both cancer and stromal tissues, and p53 protein expression was detected in both the cancer cells and the cancer stroma. Most cancer stroma in EOC is thought to originate from non-neoplastic cells, but some parts of the cancer stroma might originate from cancer cells. **Key Words:** Ovarian cancer—Stroma—*p53*.

Cancer consists of founder cancer cells and stroma, including blood and lymph endothelial cells, inflammatory cells, immunocytes, macrophages, and fibroblasts. The stroma is thought to play an important role in tumor behavior, including invasion or metastasis and response to therapy (1–3). Finak et al. (4) used laser capture microdissection (LCM) to compare gene-expression profiles of tumor stroma from 53 primary breast cancers and established a new stroma-derived prognostic predictor that stratifies disease outcome independent of the standard clinical prognostic factors or published gene expression-based predictors. We previously reported the gene-expression profile in the cancer stroma to be an independent prognostic factor in epithelial ovarian cancer (EOC) (5). Cancer-induced fibroblasts are generally thought to be derived from tissue or bone marrow (6,7), or to originate from epithelial mesenchymal transition of cancer cells. Cancer stroma had been thought to originate mainly

From the Department of Obstetrics and Gynecology (T.A., A.H., H.T., F.K., H.T., E.T., H.N., T.C., Y.I., W.Y., N.S., D.A.), School of Medicine, Keio University, Tokyo; and Department of Obstetrics and Gynecology (S.N.), Osaka City General Hospital, Osaka, Japan.

Supported in part by a Grant-in-Aid for Scientific Research on Priority Areas from the Ministry of Education, Science, and Culture, Japan (20014024), a Grant-in-Aid for Scientific Research (C) from the Ministry of Education, Science, and Culture, Japan (19591940), a Grant-in-Aid for Young Scientists (B) from the Ministry of Education, Science, and Culture, Japan (22791545), and a Grant from Osaka City General Hospital.

The authors declare no conflict of interest.

Address correspondence and reprint requests to Akira Hirasawa MD, PhD, Department of Obstetrics and Gynecology, School of Medicine, Keio University, 35 Shinanomachi, Shinjyuku-ku, Tokyo 160-8582, Japan. E-mail: hir-aki@z8.keio.jp.

DOI: 10.1097/PGP.0b013e3182518533

from tissue-marrow or bone-marrow-derived fibroblasts until Kurose et al. (8) recently demonstrated high frequencies of somatic mutations in *TP53* and *PTEN* in breast neoplastic epithelium and stroma. Patocs et al. (9) reported that *TP53* mutations in the stroma of sporadic breast cancers were associated with regional nodal metastases. In this study, we evaluated the status of the *p53* gene in both the cancer cells and the cancer stroma in EOC.

MATERIALS AND METHODS

Patients and Samples

Subjects eligible for this study had histologically confirmed EOC (excluding mucinous and clear cell types). The study was approved by the institutional review board of the Osaka City General Hospital and School of Medicine, Keio University, and written informed consent was obtained from all patients. Specimens obtained at operation were immediately stored at −80°C.

LCM and DNA Extraction

LCM was performed as described previously (10,11). In brief, frozen sections (6 μm) prepared from tumor tissue specimens were affixed to 4-μm-thin Laser Microdissection Film glass slides (PALM Micolaser Technologies GmbH, Bernried, Germany) and stained using the Histogene LCM Frozen Section Staining Kit (Arcturus Engineering, Mountain View, CA). Stained sections were microdissected using a PixCell IIe LCM system (Arcturus Engineering). Tumor cells and adjacent nontumor stromal cells were visualized under the microscope and selectively detached by activation of the laser. Dissected stromal tissues were located within 200 cells of the margin of tumors. DNA extraction was performed using the PicoPure DNA Extraction Kit according to the manufacturer's instructions (Arcturus Engineering).

Polymerase Chain Reaction (PCR) Amplification of p53 Gene and Sequence Analysis

We analyzed *p53* sequences (exons 5–8) of both cancer and stromal tissues in 16 cases. To amplify exons 5, 6, and 8 of the *p53* gene, we performed PCR; only exon 7 was amplified with nested PCR using whole aliquots of DNA (12,13). Primer sequences were as follows: exons 5-6, 5′-GTTTCTTTGCTGC CGTCTTC-3′ (sense) and 5′-TTGCACATCTCAT GGGGTTA-3′ (antisense); exon 8, 5′-GGTAGGA CCTGATTTCCTTACTGCC-3′ (sense) and 5′-CCC TTGGTCTCCTCCACCGTCTCTTG-3′ (antisense); exon 7 first, 5′-GCGGTCCCAAAAGGGTCAGT CCCTGCTTGCCACAGGTC-3′ (sense) and 5′-GC GGTCCCAAAAGGGTCAGTAAGAAATCGGTA AGAGGTGGG-3′ (antisense); exon 7 second, 5′-CCAAGGCGCACTGGCCTC-3′ (sense) and 5′-TGGGGCACAGCAGGCCAG-3′ (antisense). PCR products were then subjected to electrophoresis on 2% agarose gel. Direct sequencing was performed using the ABI PRISM Big Dye Terminator Ver3.1 Cycle Sequencing Kit according to the manufacturer's instructions on an ABI PRISM 3100 (Applied Biosystems, Foster City, CA). PCR amplification and sequence using the same primers. The sequences were compared with the published wild-type sequences (http://getentry.ddbj.nig.ac.jp).

Immunohistochemistry of p53 Protein

We examined the expression of p53 protein in 16 cases. Formalin-fixed, paraffin-embedded tissues were cut into 4-μm sections. Sections were deparaffinized in xylene and 100% ethanol for 5 min each, followed by washing in water. Antigen retrieval was accomplished by autoclave in sodium citrate buffer (10 mM, pH 6.0) at 121°C for 10 min. The sections were then incubated in methanol containing 3% hydrogen peroxide for 30 min at room temperature to quench endogenous peroxidase activity. Sections were rinsed in phosphate-buffered saline and incubated with the primary antibody, anti-human p53 (DO7) mouse monoclonal antibody (Dako, Glostrup Denmark), at 4°C overnight. The sections were washed in phosphate-buffered saline and EnVision+ Peroxidase (Dako), and then incubated for 30 min at room temperature. p53-positive staining was visualized by applying a 3,3′-diaminobenzidine chromogen containing 0.05% hydrogen peroxidase for 5 min at room temperature. Nuclei were counterstained using Mayer's hematoxylin. Negative controls not exposed to the primary antibody were included in all experiments. Positive and negative tumor-staining controls were included.

RESULTS

Patients' Backgrounds

The samples were obtained from 16 EOC patients with a median age of 55 yr (range, 34–72 yr). One sample was Stage I, 3 were Stage II, 7 were Stage III, and 5 were Stage IV; 5 were Grade G1, 4 were Grade 2, and 7 were Grade 3. Five tumors were endometrioid, 8 serous, and 3 of undifferentiated type.

Status of *p53* Gene and p53 Protein

p53 mutations and p53 protein expression were examined in 16 cases (Table 1). *p53* mutations were detected in 9 cases, in 8 of which the mutations were present only in the cancer cells. In case 3, the same mutation (R248Q) was detected in both cancer and stromal tissues, but not in the normal uterine tissue of the patient (Fig. 1). The *p53* mutation is present in cancer (Fig. 1A), and the *p53* mutant is the dominant allele in the stromal samples (Fig. 1B, C) but not the uterine tissue (Fig. 1D). This case was stage 3c endometrioid adenocarcinoma with lymph node metastasis.

Among the 16 cases examined, p53 protein expression was detected in the cancer cells of 9 cases and the stromal tissues of 2 cases. Of the 9 cases with p53 protein expression in cancer tissue, 5 had *p53* mutations, and of the 7 cases without p53 protein expression in cancer tissue, 4 had *p53* mutations. Case 7 had p53 protein expression in both cancer and stromal tissues, with no *p53* mutation. In contrast, case 3 had a *p53* gene mutation and p53 protein expression in both cancer and stromal tissues (Figs. 2A, B). The stromal cells expressing p53 were adjacent to the border between the cancer cells and the cancer stroma.

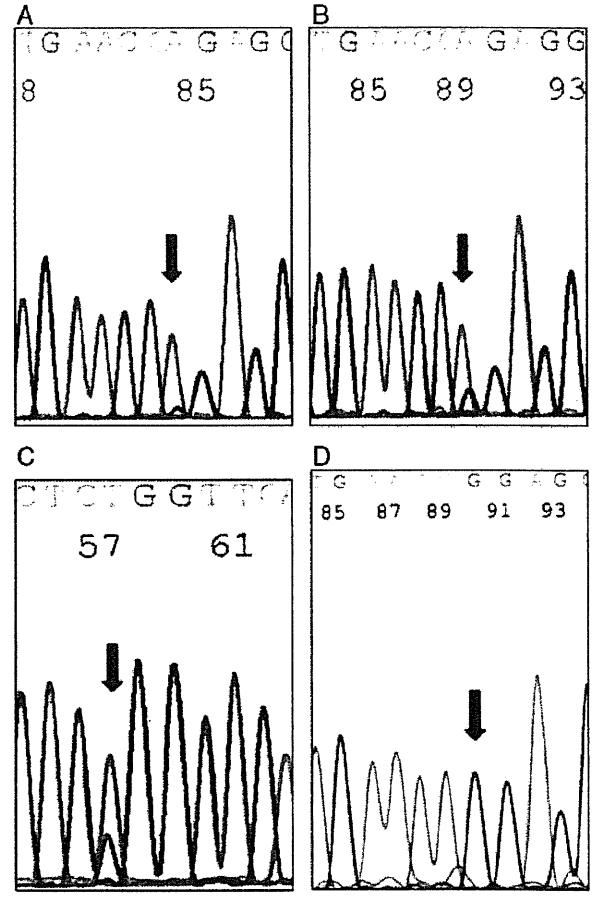

FIG. 1. *p53* gene mutation: in case 3, the *p53* gene mutation is present in cancer cells (A) and stromal cells (B, C) but not detected in the uterine tissue (D).

DISCUSSION

We evaluated *p53* mutations separately in cancer and stromal cells of 16 EOCs to elucidate the origin of cancer stroma. Mutations in *p53* were detected in 9 of 16 EOCs, and in 8 of these cases, the mutations were detected in only cancer cells. Cancer-induced fibroblasts are generally thought to either be non-neoplastic cells, including tissue-marrow or bone-marrow-derived fibroblasts (6,7), or originate from epithelial mesenchymal

TABLE 1. *Immunolocalization of p53 protein and p53 gene status in 16 cases*

Case	Age	HIS	ST	GR	*p53* cancer	*p53* stroma	*p53* uterus	p53 IHC cancer	p53 IHC stroma
1	70	EC	2c	3	Wild	Wild	ND	+	–
2	66	EC	3c	1	C176Y	Wild	ND	+	–
3	66	EC	3c	1	R248Q	R248Q	Wild	+	+
4	55	EC	4	3	Wild	Wild	ND	+	+
5	54	EC	4	3	P278L	Wild	ND	–	–
6	61	SC	1cb	2	Wild	Wild	ND	+	–
7	53	SC	2a	1	F212del	Wild	ND	–	–
8	49	SC	2c	2	Wild	Wild	ND	–	–
9	34	SC	3c	1	L194H	Wild	ND	+	–
10	59	SC	3c	2	R306stop	Wild	ND	–	–
11	63	SC	4	3	E171stop	Wild	ND	–	–
12	57	SC	4	2	Wild	Wild	ND	–	–
13	53	SC	3c	1	H273R	Wild	ND	+	–
14	61	UD	3c	3	Wild	Wild	ND	+	–
15	51	UD	3c	3	V216M	Wild	ND	+	–
16	72	UD	4	3	Wild	Wild	ND	–	–

EC indicates endometrioid adenocarcinoma; GR, histologic grade; HIS, histology; IHC, immunohistochemistry; ND, not done; SC, serous cystadenocarcinoma; ST, FIGO stage; UD, undifferentiated carcinoma.

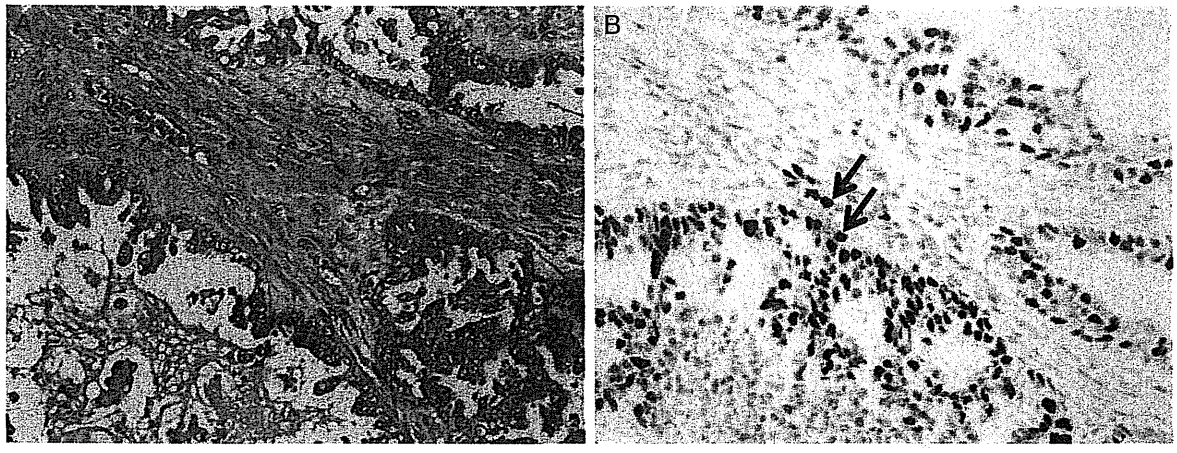

FIG. 2. Hematoxylin-eosin stain and p53 protein expression in case 3. (A, B) In case 3, p53 protein was detected in both cancer cells and stromal cells near the border between the cancer cells and the cancer stroma [(B); arrows].

transition of cancer cells. At present, tissue-marrow or bone-marrow-derived fibroblasts are thought to be more common. In our study, the cancer stroma of EOC seems to derive from non-neoplastic tissues in 8 of 9 *p53* mutant cases.

However, there was 1 case where the same mutation (R248Q) was detected in both cancer and stromal tissues, but not in normal uterine tissue of the patient. Furthermore, p53 protein expression was detected in both the cancer cells and the cancer stroma, and the p53-expressing stromal cells were near the border between cancer cells and cancer stroma. There are at least 2 possible interpretations: it may be that in this case, some part of the cancer stroma originated from cancer cells; alternatively, although we carefully used the LCM technique, there could have been cross-contamination between the 2 compartments. However, the latter seems unlikely because the p53 protein was detected in both the cancer cells and the cancer stroma. In breast cancer, high frequencies of somatic mutations in *TP53* and *PTEN* have been detected in breast neoplastic epithelium and stroma, and *TP53* mutations in the stroma of sporadic breast cancers are associated with regional nodal metastasis (8,9). However, Qiu et al. (14) showed that the loss of heterozygosity and copy number alterations are extremely rare in cancer-associated fibroblasts of ovarian cancer. Recently, Kato et al. (15) isolated and characterized side-population cells from human endometrial cancer. They demonstrated that side-population cells form large, invasive tumors composed of both tumor cells and stromal-like cells, and that the stromal-like cells were derived from the inoculated tumor cells.

In 1 case, p53 protein expression was detected in both the cancer cells and the stroma, but no *p53* mutations were detected in either. In 4 cases, p53 protein expression was detected in the cancer cells, but *p53* mutations were not detected. We had expected *p53* gene mutations to be related to p53 protein expression but found *p53* gene mutations to not always be accompanied with p53 protein expression (16). The p53 protein may accumulate from other factors such as cellular insults or hypoxia, or by forming complexes with other molecules such as PMDM2 (17–19).

In conclusion, most cancer stroma of EOC is thought to originate from non-neoplastic cells but some parts might originate from cancer cells.

REFERENCES

1. Bhowmick NA, Moses HL. Tumor-stroma interactions. *Curr Opin Genet Dev* 2005;15:97–101.
2. Kim JB, Stein R, O'Hare MJ. Tumour-stromal interactions in breast cancer: the role of stroma in tumourigenesis. *Tumour Biol* 2005;26:173–85.
3. Tlsty TD, Coussens LM. Tumor stroma and regulation of cancer development. *Annu Rev Pathol* 2006;1:119–50.
4. Finak G, Bertos N, Pepin F, et al. Stromal gene expression predicts clinical outcome in breast cancer. *Nat Med* 2008;14: 518–27.
5. Kataoka F, Tsuda H, Arao T, et al. EGR1 and FOSB gene expression in cancer stroma are independent prognostic indicators for epithelial ovarian cancer receiving standard therapy. *Genes Chromosomes Cancer* 2012;51:300–12.
6. Ishii G, Ito TK, Aoyagi K, et al. Presence of human circulating progenitor cells for cancer stromal fibroblasts in the blood of lung cancer patients. *Stem Cells* 2007;25:1469–77.
7. Chiba H, Ishii G, Ito TK, et al. CD105-positive cells in pulmonary arterial blood of adult human lung cancer patients include mesenchymal progenitors. *Stem Cells* 2008;26: 2523–30.

8. Kurose K, Gilley K, Matsumoto S, et al. Frequent somatic mutations in PTEN and TP53 are mutually exclusive in the stroma of breast carcinomas. *Nat Genet* 2002;32:355–57.
9. Patocs A, Zhang L, Xu Y, et al. Breast-cancer stromal cells with TP53 mutations and nodal metastases. *N Engl J Med* 2007;357:2543–51.
10. Tsuda H, Birrer MJ, Ito YM, et al. Identification of DNA copy number changes in microdissected serous ovarian cancer tissue using a cDNA microarray platform. *Cancer Genet Cytogenet* 2004;155:97–107.
11. Tsuda H, Ito YM, Ohashi Y, et al. Identification of overexpression and amplification of ABCF2 in clear cell ovarian adenocarcinomas by cDNA microarray analyses. *Clin Cancer Res* 2005;11:6880–8.
12. Heinmoller E, Liu Q, Sun Y, et al. Toward efficient analysis of mutations in single cells from ethanol-fixed, paraffin-embedded, and immunohistochemically stained tissues. *Lab Invest* 2002;82:443–53.
13. Akahane T, Sekizawa A, Purwosunu Y, et al. The role of p53 mutation in the carcinomas arising from endometriosis. *Int J Gynecol Pathol* 2007;26:345–51.
14. Qiu W, Hu M, Sridhar A, et al. No evidence of clonal somatic genetic alterations in cancer-associated fibroblasts from human breast and ovarian carcinomas. *Nat Genet* 2008;40:650–55.
15. Kato K, Takao T, Kuboyama A, et al. Endometrial cancer side-population cells show prominent migration and have a potential to differentiate into the mesenchymal cell lineage. *Am J Pathol* 2010;176:381–92.
16. Hashiguchi Y, Tsuda H, Yamamoto K, et al. Combined analysis of p53 and RB pathways in epithelial ovarian cancer. *Hum Pathol* 2001;32:988–96.
17. Hall PA, McKee PH, Menage HD, et al. High levels of p53 protein in UV-irradiated normal human skin. *Oncogene* 1993;8:203–7.
18. Graeber TG, Osmanian C, Jacks T, et al. Hypoxia-mediated selection of cells with diminished apoptotic potential in solid tumours. *Nature* 1996;379:88–91.
19. Momand J, Zambetti GP, Olson DC, et al. The mdm-2 oncogene product forms a complex with the p53 protein and inhibits p53-mediated transactivation. *Cell* 1992;69:1237–45.

J. Biochem. 2012;152(6):587–594 doi:10.1093/jb/mvs112

JB THE JOURNAL OF BIOCHEMISTRY

Possible involvement of glycolipids in anticancer drug resistance of human ovarian serous carcinoma-derived cells

Received July 5, 2012; accepted August 28, 2012; published online October 4, 2012

Kyoko Tanaka[1], Hidetaka Takada[2], Seiji Isonishi[3], Daisuke Aoki[1], Mikio Mikami[4], Kazushige Kiguchi[5] and Masao Iwamori[2,*]

[1]Department of Obstetrics and Gynecology, School of Medicine, Keio University, 35 Shinanomachi, Shinjuku-ku, Tokyo 160-8582, Japan; [2]Department of Biochemistry, Faculty of Science and Technology, Kinki University, 3-4-1 Kowakae, Higashiosaka, Osaka 577-8502, Japan; [3]Department of Obstetrics and Gynecology, Jikei University School of Medicine, Daisan Hospital, 4-11-1 Izumihoncho, Komae, Tokyo 201-8601, Japan; [4]Department of Obstetrics and Gynecology, Tokai University School of Medicine, 143 Shimokasuya, Isehara, Kanagawa 259-1193, Japan; and [5]Department of Obstetrics and Gynecology, St. Marianna University School of Medicine, 2-16-1 Sugao, Miyamae-ku, Kawasaki, Kanagawa 216-8511, Japan

*Masao Iwamori, Department of Biochemistry, Faculty of Science and Technology, Kinki University, 3-4-1 Kowakae, Higashiosaka, Osaka 577-8502, Japan. Tel: +81-6-6721-2332, Fax: +81-6-6723-6721, email: iwamori@life.kindai.ac.jp

Glycolipid and transporter protein gene expression in ovarian serous carcinoma-derived 2008 cells, and their paclitaxel-resistant Px2 and cisplatin-resistant C13 forms was examined to confirm the previous finding, i.e., that it was characteristically altered in anticancer drug-resistant cells established on continuous cultivation of ovarian carcinoma-derived KF28 cells in the different anticancer drug-containing media. Although the concentrations of lipid constituents in 2008 cells were higher than those in KF28 cells, and the glycolipid compositions were different, the following glycolipids and genes were commonly altered in KF28- and 2008-derived resistant cells. Gb_3Cer was increased in all resistant cells, irrespective of whether the resistance was to paclitaxel or cisplatin, and expression of the MDR1 gene and gangliosides was enhanced in paclitaxel-resistant cells, but gangliosides were absent in cisplatin-resistant cells. In accord with the decreased amounts of gangliosides in cisplatin-resistant cells, the gene expression and specific activity of GM3 synthase were greatly decreased in cisplatin-resistant cells. Furthermore, paclitaxel- and cisplatin-resistant cells were converted to forms more sensitive to the respective anticancer drugs on cultivation with D-PDMP, an inhibitor of GlcCer synthase, and GM3, respectively, prior to the addition of anticancer drugs, indicating the possible involvement of glycolipids in anticancer drug resistance.

Keywords: anticancer drugs/gangliosides/glycolipids/ovarian carcinoma/sialyltransferase.

Abbreviations: ABC, ATP-binding cassette; BSA, bovine serum albumin; CMH, ceramide monohexoside; MDR, multidrug resistance; MRP, multidrug resistance-associated protein; PDMP, 1-phenyl-2-decanoylamino-3-morpholino-1-propanol.

Glycosphingolipids are amphipathic molecules consisting of hydrophobic ceramide and hydrophilic carbohydrate moieties, and are ubiquitously distributed in tissues and cells [The glycolipid nomenclature is based on the recommendations of the IUPAC-IUB Commission on Biochemical Nomenclature (*1*).]. Their carbohydrate structures characteristically change in association with cellular differentiation and transformation, mainly due to the aberrant expression of glycosyl transferases, and among the transformation-associated carbohydrates, a sialylated lacto-N-fucopentaose (sialyl Le^a) has been successfully applied for the clinical diagnosis of cancer patients (*2*, *3*). Also, on the basis of the finding that sialylated or sulfated Lewis carbohydrates are included in the ligands for selectins (*4*, *5*), detection of related carbohydrates in sera of patients has been performed to determine the metastatic potential of a cancer (*6*, *7*). On the other hand, ceramide has been characterized as a signal mediator for several cellular events, i.e., stress responses to heat, UV-irradiation and hypoxia, and apoptosis caused by chemotherapeutic agents (*8*), during which ceramide is generated from sphingomyelin by acid sphingomyelinase as an initial event of signal transduction (*9*). Also, enhanced glycolipid synthesis on transfection with the ceramide glucosyltransferase gene has been revealed to abolish ceramide-dependent apoptosis, probably through conversion of ceramide generated from sphingomyelin into glycolipids, which yields cells exhibiting greater resistance to anticancer drugs (*10*). However, since the cellular distribution of sphingomyelinase is different from that of glycosyltransferase, it is unclear whether or not ceramides derived from sphingomyelin are really converted into GlcCer in the signal transduction cascade (*11*). In fact, that anticancer drug-sensitivity is irrelevant as to the synthetic potential for glycolipids has been reported for neuroblastoma, leukemia and melanoma cells (*12*, *13*).

In our previous studies, when ovarian serous carcinoma-derived KF28 cells were compared with their anticancer drug-resistant KF28TX, KFr13 and KFr13TX forms, the resistant cells were found to express transporter genes, i.e., characteristic expression of MDR1 in paclitaxel-resistant KF28TX and KFr13TX cells, and enhanced expression of MRP2 in cisplatin-resistant KFr13 and KFr13TX ones. In

addition, although no significant differences in the amounts of ceramide and sphingomyelin were observed between them, Gb_3Cer was increased in both paclitaxel- and cisplatin-resistant cells, and GM3 was increased in the paclitaxel-resistant cells, but was absent in the cisplatin-resistant ones (*14*, *15*), suggesting that glycolipids together with transporter proteins are necessary for the survival of cells in anticancer drug-containing media, probably through regulation of the activity of transporters by both the carbohydrate and ceramide moieties of glycolipids in membrane rafts (*16*). To further characterize the glycolipids associated with anticancer drug resistance, we determined the glycolipid compositions and gene expression of transporters in ovarian serous carcinoma-derived 2008 cells (*17*), and paclitaxel-resistant Px2 and cisplatin-resistant C13 cells (*18*, *19*), and examined the effects of D-PDMP, an inhibitor of GlcCer synthase, and of exogenous addition of GM3 on the anticancer drug resistance of KF28- and 2008-derived cells, and their anticancer drug-resistant forms.

Materials and Methods

Materials

Sphingolipids from various sources were purified in our laboratory: GlcCer, LacCer, Gb_3Cer, Gb_4Cer, nLc_4Cer and GM3 from human erythrocytes, and GalCer and sphingomyelin from bovine brain, and their N-stearoyl derivatives were prepared by deacylation with sphingolipid ceramide N-deacylase (*Pseudomonas sp.* TK4), followed by reacylation with stearoyl chloride. Ceramides were prepared by treatment of sphingomyelin with *Clostridium perfringens* phospholipase C. The following monoclonal antibodies were kindly donated: MSN-1 towards Le^a plus Le^b by Dr S. Nozawa, Keio University, Tokyo, 3C11 towards sialyl Le^a by Dr K. Matsumoto, Mikuri Immunol. Lab., Kyoto, YHD-06 towards GM2 by Dr M. Yamazaki, Konica Co., Tokyo, and M2590 towards GM3, and anti-Gb_3Cer and anti-Gg_3Cer antibodies by Seikagaku Co., Tokyo. Peroxidase-conjugated anti-mouse IgG, A and M antibodies, peroxidase-conjugated-cholera toxin B-subunit and sialidase (*V. cholerae*) were purchased from Sigma Aldrich, St. Louis, MO, USA. The inhibitor of ceramide glucosyltransferase, D-threo-1-phenyl-2-decanoylamino-3-morpholino-1-propanol (D-PDMP), and its L-isomer were kindly donated by Dr J. Inokuchi, Tohoku Pharmaceutical University, Sendai. Cisplatin and paclitaxel were obtained from Bristol-Myers Squibb Co., Tokyo.

Cell lines

Ovarian serous carcinoma-derived 2008 and KF28 cells, and paclitaxel-resistant Px2 and KF28TX cells, and cisplatin-resistant C13 cells and KFr13 cells were used in this experiment. PRM1-1640 and DMEM media supplemented with 10% FCS, 100 U/ml penicillin and 0.1 mg/ml streptomycin were the media for 2008, Px2 and C13 cells, and for KF28, KF28TX and KFr13 cells, respectively, which were cultured in a humidified incubator at 37°C under a 5% CO_2 atmosphere (*17–19*). At every subculture step, Px2 and KF28TX, and C13 and KFr13 cells were cultured in media containing 0.1 μg/ml paclitaxel and 0.3 μg/ml cisplatin, respectively, for 2 h before the addition of 0.05% trypsin and 0.02% EDTA.

Cell viability in media containing anticancer drugs

Cells (1×10^4) cultured in 96-well plates for 24 h were exposed to various concentrations (0.0001 ~ 20 μg/ml) of paclitaxel or cisplatin for a further 48 h, followed by culture in the medium containing MTT (3(4,5-dimethyl-2-thiazolyl)-2,5-dimethyl-2 H-tetrasolium bromide, 1 μg/μl) for 4 h. The resultant formazan pigment was dissolved with dimethyl sulfoxide, and then the optical density was determined at 560 nm (*14*). Also, cells were cultured in the medium containing D- and L-PDMP or GM3 at the concentration of 10 μM for 48 h prior to exposure to anticancer drugs.

Separation and quantitation of lipids

After extraction of the total lipids from lyophilized cells, the concentrations of cholesterol, ceramide and phospholipids in the lipid extracts were determined by TLC-densitometry with n-hexane/diethyl ether/acetic acid (80:30:2, v/v/v), chloroform/methanol/acetic acid (94:1:5, v/v/v) and chloroform/methanol/water (60:35:8, v/v/v), respectively, followed by visualization with cupric acetate-phosphoric acid reagent. Then, the lipid extracts were fractionated into neutral and acidic lipids on a DEAE-Sephadex column (A-25, acetate form; Pharmacia, Uppsala, Sweden), and neutral glycolipids and gangliosides were prepared from the neutral and acidic lipids as described previously (*14*, *15*). The gangliosides and neutral glycolipids thus obtained were separated by TLC with chloroform/methanol/0.5% $CaCl_2$ in water (55:45:10, v/v/v) and chloroform/methanol/water (60:35:8, v/v/v), and then visualized with resorcinol-HCl and orcinol-H_2SO_4 reagents, respectively. Standard glycolipids: N-stearoyl derivatives of GalCer, LacCer, Gb_3Cer and GM3 (0.1–1.5 μg) were developed on the same TLC plates for the preparation of standard curves. The glycolipids were also detected by TLC-immunostaining as described previously (*14*, *15*), and for characterization of ganglioside GD1a, after blocking, the plate was incubated with neuraminidase (20 mU) in PBS at 37°C for 1 h, and then stained with peroxidase-conjugated cholera toxin B-subunit (1:500) at room temperature for 30 min.

RT-PCR analysis

Total RNA extracted from the cell lines by the acid guanidine thiocyanate-phenol-chloroform (AGPC) method was reverse-transcribed to cDNA with reverse transcriptase (M-MuLV; Takara, Kyoto) and random primers, and then subjected to PCR under the following conditions: MDR1 (GenBank Accession Number AF016535), sense primer, cccatcattgcaatagcagg, antisense primer, gttcaaacttctgctcctga; MRP1 (NM004996), sense primer, atgtcacgtggaataccagc, antisense primer, gaagactgaactcccttcct; MRP2 (NM000392), sense primer, ctgcctcttcagaatcttag, antisense primer, ataacccaagttgcaggct; ceramide glucosyltransferase (Glc T, NM003358), sense primer, caaaactctggctcatattc, antisense primer, atattgtcatggattcgcgg; ceramide galactosyltransferase (Gal T, NM003360), sense primer, ctctctgaaggcagagacatcgcc, antisense primer, catccacaggctggacccatgaac; and LacCer sialyltransferase (GM3 synthase, AB018356), sense primer, atttgagcacaggtatagc, antisense primer, gatgtcaaaggcagtctct, 35 cycles of 95°C for 15 s, 52–64°C for 30 s, and 72°C for 40 s. The primers for glyceraldehyde 3-phosphate dehydrogenase (GAPDH) were used as controls. The resulting PCR products were electrophoresed on a 1.5% agarose gel, stained with ethidium bromide, and then examined under a UV transilluminator.

GM3 synthase activity

Cells were homogenized in 0.25 M sucrose with a Potter-Elvehjem homogenizer to prepare 10% (w/v) homogenates, which were then centrifuged at 1,000 × g for 10 min at 4°C to remove cell debris, followed by centrifugation at 100,000 × g for 60 min to obtain cytosol and microsomal fractions. Each microsomal fraction was suspended in 0.25 M sucrose by sonication and its protein concentration was measured by the protein dye binding method with BSA as the standard (*20*). The standard assay mixture comprised 5 μg LacCer, 10 mM $MgCl_2$, 5 mM $CaCl_2$, 0.3% Triton CF-54, 10 mM CMP-[4-^{14}C]NeuAc (67 μBq/mmol), 50 mM 4-morpholinoethane sulfonic acid buffer (pH 6.4) and 50–100 μg enzyme protein, in a final volume of 50 μl. After incubation at 37°C for 2 h, the reaction was stopped with 150 μl of methanol, and the products were separated by hydrophobic chromatography with a Sep-pak cartridge (C18; Waters Associates, Milford, MA), followed by TLC with chloroform/methanol/0.5% $CaCl_2$ in water (55:45:10, v/v/v). The TLC plate was exposed to an X-ray film (RX-U, Fuji, Tokyo) and the radioactivity incorporated into GM3 was determined using a liquid scintillation counter (Tri-Carb 1500; Packard, Foster City, CA).

Structural analysis of glycolipids

Purification of individual glycolipids was performed by silica gel (Iatrobeads 6RS8060; Iatron Laboratory, Tokyo) column chromatography as described previously (*14*, *15*). The purified glycolipids were identified by negative ion FABMS (JMS-700TKM; JEOL, Tokyo) with triethanolamine as a matrix solvent, and their fatty

acid and long chain base compositions were determined by GC-mass spectrometry (GP5050; Shimadzu, Kyoto) on a DB-1 column (0.25 mmø × 30 m) as their methyl ester and aldehyde derivatives, respectively (*21*).

Results

Ovarian serous carcinoma-derived KF28 and 2008 cells, and their anticancer drug-resistant forms

Paclitaxel-resistant KF28TX and Px2, and cisplatin-resistant KFr13 and C13 cells well retained their resistance against the respective drugs. As shown in Table I, the IC50s of paclitaxel for KF28TX and Px2 cells, and of cisplatin for KFr13 and C13 cells were about 10-fold and about 6-fold those for the parent cells, respectively. As to ABC-transporter proteins, although no significant difference was observed in the gene expression of MRP1 or MRP2 between the parent 2008 cells and the resistant ones, the relative expression of the MDR1 gene in the paclitaxel-resistant Px2 cells was higher than that in the parent 2008 and cisplatin-resistant C13 ones (Fig. 1), and these findings were in accord with our previous observations for KF28-derived resistant ones (*14*).

Lipids in ovarian carcinoma-derived KF28 and 2008 cells, and their anticancer drug-resistant forms

When the lipid compositions of ovarian carcinoma-derived KF28 and 2008 cells were compared, the amounts of cholesterol and phospholipids in 2008 cells were found to be 2- to 3-fold those in KF28 ones, probably due to the smaller cell size of 2008 cells than that of KF28 ones, but the relative ratio of total phospholipids to cholesterol were similar in the two types of cells, being 1.2 for KF28 and 1.6 for 2008 cells, respectively (Table II and Fig. 2) (*14*). But, the glycolipid composition in 2008 cells was distinctly different from that in KF28 cells. The major glycolipids present at more than 0.02 μg per mg dry weight in 2008 cells were LacCer, CMH, Gb_3Cer, Gg_3Cer, GM3, GM2, Le^b and GM1, whereas those in KF28 cells were CMH and GM3 (Figs. 2 and 3). Thus, 2008 cells showed a more complex glycolipid composition than KF28 ones, the occurrence of GM1, a component in human neural cells, being a particularly notable character of 2008 cells (Fig. 4).

As to 2008-derived anticancer drug-resistant cells, the amounts of cholesterol and total phospholipids in both paclitaxel-resistant Px2 and cisplatin-resistant C13 cells were similar to those in the original 2008 cells, but the amounts of glycolipids were dramatically different in the resistant ones (Fig. 3). Gb_3Cer and Gg_3Cer, whose structures were confirmed by their reactivities with anti-Gb_3Cer and anti-Gg_3Cer antibodies, respectively, in both Px2 and C13 cells were 3- and 2-fold those in the parent 2008 cells, respectively, comprising 32, 58 and 74% of the total neutral glycolipids in 2008, Px2 and C13 cells, respectively (Fig. 4 and Table II). Thus, trihexaosyl ceramides, particularly Gb_3Cer, were characteristically increased in both Px2 and C13 cells, irrespective of whether the resistance was to paclitaxel or cisplatin, and these findings were in accord with our previous observations for KF28-derived resistant ones (Fig. 2) (*14*).

Also, the increased amount of gangliosides in the paclitaxel-resistant cells and their absence in the cisplatin-resistant ones, in comparison to those in KF28 cells, were similarly observed in 2008-derived Px2 and C13 cells, respectively. However, in contrast to that KF28 cells contained GM3 as the sole ganglioside, which was increased in paclitaxel-resistant KF28TX cells (*14*), 2008 cells contained GM3, GM2 and GM1, whose amounts, together with that of GD1a, in Px2 cells were more than 4-fold those in the parent 2008 cells (Figs. 3 and 4, and Table II). The structures of GM3 and GM2 were confirmed by their reactivities with anti-GM3 and anti-GM2 antibodies, respectively, and that of GM1 with anti-GM1 antibodies and cholera toxin (Fig. 4). Also, GD1a was confirmed by the staining with cholera toxin B subunit after neuraminidase treatment (Fig. 4H) and negative ion FABMS, on which molecular ions, m/z 1835 for the 18:0-containing one and m/z1917 for the 24:1-containing one, as the major molecular species, and fragment ions corresponding to GM1, GM2, Gg_3Cer, LacCer, CMH and ceramides were yielded, as reported previously (*22*).

Although GM1 was not detected in 0.05 mg dry weight of C13 cells on immunostaining with anti-GM1 antibodies, whose detection limit for GM1 is about 5 ng (Fig. 4G), it was revealed to be present in C13 cells on staining with cholera toxin, which detects more than 1 pg of GM1, the amount of GM1 in C13 cells being estimated to be about 1 ng per mg dry weight (trace amount in Table II). As shown in Table II, the rates of increase of GM1 and GD1a in Px2 cells in comparison to those in 2008 cells were higher than those of GM3 and GM2. Also, sialyl Le^a was found to be present only in Px2 cells, i.e., not in 2008 or C13 cells. Thus, the total negative charge due to sialic acid in gangliosides in Px2 and C13 cells was more than 10-fold and less than one-hundredth of that in 2008 cells, respectively. On the other hand, although the proportion of 2-hydroxy fatty acid-containing glycolipids was characteristically increased in KF28-derived resistant cells (*15*), no significant changes in the fatty acid and long chain base compositions of glycolipids were observed between anticancer drug-sensitive 2008 cells, and resistant Px2 and C13 ones, the major molecular species being 16:0-, 18:0-, 22:0-, 24:0- and 24:1-containing ones.

GM3 synthase activity

On RT-PCR, the ceramide glucosyltransferase and galactosyltransferase genes were found to be intensely expressed in all cells, but the relative intensity of the GM3 synthase gene was higher in Px2 cells and lower in C13 cells than in 2008 cells (Fig. 1). Also, enhanced and attenuated expression of the GM3 synthase gene was observed in KF28TX and KFr13 cells, respectively, as reported previously (*14*). To examine the correlation between gene expression and enzyme activity, GM3 synthase activity in the microsomal fraction was determined with CMP-[4-^{14}C]NeuAc and LacCer as the substrates. As shown in Fig. 5 and Table III, the

Table I. Sensitivity to paclitaxel and cisplatin of ovarian carcinoma-derived cells and their anticancer drug-resistant forms.

Cells	IC50 concentration (μg/ml)	
	Paclitaxel	Cisplatin
KF28	0.12 ± 0.03	0.90 ± 0.02
KF28TX	1.22 ± 0.05	0.11 ± 0.02
KFr13	0.20 ± 0.02	5.54 ± 0.11
2008	0.10 ± 0.03	1.02 ± 0.05
Px2	0.95 ± 0.06	0.97 ± 0.03
C13	0.15 ± 0.03	5.95 ± 0.20

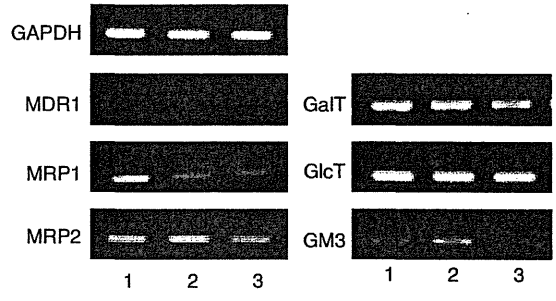

Fig. 1 RT-PCR analysis of transporter proteins and glycosyltransferase genes. 1, ovarian carcinoma-derived 2008 cells; 2, paclitaxel-resistant Px2 cells; and 3, cisplatin-resistant C13 cells. GalT, ceramide β-galactosyltransferase; GlcT, ceramide β-glucosyltransferase; and GM3, LacCer sialyltransferase.

Table II. Lipid compositions of human ovarian carcinoma-derived 2008 cells, and taxol-resistant Px2 and cisplatin-resistant C13 ones (μg per mg dry weight).

Lipid	2008	Px2	C13
Cholesterol	10.8 ± 0.6	10.9 ± 0.4	9.3 ± 0.5
PE	5.9 ± 0.7	4.9 ± 0.9	6.0 ± 0.7
PG	1.0 ± 0.2	0.9 ± 0.3	1.1 ± 0.4
PC/PS	8.6 ± 1.4	8.4 ± 1.6	7.9 ± 1.3
SM	1.7 ± 0.4	1.6 ± 0.3	2.1 ± 0.4
Ceramide	1.70 ± 0.09	1.61 ± 0.03	1.57 ± 0.06
CMH	0.60 ± 0.06	0.49 ± 0.07	0.35 ± 0.07
LacCer	0.92 ± 0.08	0.66 ± 0.08	0.10 ± 0.01
Gb_3Cer	0.45 ± 0.03	1.35 ± 0.04	1.57 ± 0.05
Gg_3Cer	0.26 ± 0.03	0.48 ± 0.03	0.58 ± 0.04
Gb_4Cer	–	0.16 ± 0.02	0.30 ± 0.06
Le^a	0.01	0.03	–
Le^b	0.03	0.02	–
GM3	0.05	0.21	–
GM2	0.03	0.33	–
GM1	0.02	0.33	tr
GD1a	–	0.22	–
Sialyl Le^a	–	0.14	–

Values are the means for individual lipids in four different experiments.
tr, trace amount (<0.005 μg/mg dry weight); –, not detected; PE, phosphatidyl ethanolamine; PG, phosphatidyl glycerol; PC, phosphatidyl choline; PS, phosphatidyl serine; and SM, sphingomyelin.

activity was detected in both KF28 and 2008 cells, and their paclitaxel-resistant forms, whose activities were not closely correlated with the relative intensity of the gene, but there were only trace levels in their cisplatin-resistant forms.

Effects of PDMP and GM3 on anticancer drug-resistance

To further characterize the possible involvement of glycolipids in anticancer drug resistance, KF28, KF28TX and KFr13 cells were cultured in media containing D- and L-PDMP, and GM3 at the concentration of 10 μM for 48 h, prior to the addition of anticancer drugs. KF28TX cells treated with D-PDMP were converted into ones more sensitive to paclitaxel than those without treatment (Fig. 6A), but no significant effect on paclitaxel sensitivity was observed in the following cells, KF28TX with either L-PDMP or GM3, and KF28 and KFr13 cells with any of D-PDMP, L-PDMP or GM3. While KFr13 cells treated with GM3, but not with D- or L-PDMP, became more sensitive to cisplatin (Fig. 6B), an effect of GM3 on cisplatin sensitivity was not clearly observed in KF28 or KF28TX cells.

To evaluate the effects of D-PDMP and exogenous GM3 on the amounts of glycolipids in KF28, KF28TX and KFr13 cells, the relative amounts of Gb_3Cer and GM3 were examined by TLC-immunostaining, as shown in Fig. 7. Gb_3Cer and GM3 in KF28TX cells after treatment with D-PDMP were reduced to 25% and 45% of the levels in KF28TX cells, respectively, but no significant change in MDR1 gene expression was observed in KF28TX cells after treatment with D-PDMP. Consequently, although MDR1 gene expression was essential for the paclitaxel resistance, the reduced amounts of glycolipids, particularly of Gb_3Cer and GM3, were thought to be involved in the decreased activity of the transporter proteins in the glycolipid-rich membrane rafts, resulting in the conversion of KF28TX cells into ones with a more responsive character as to paclitaxel. On the other hand, GM3 was undetectable in the cisplatin-resistant KFr13 cells, in which GM3 after incubation with exogenous GM3 was present in a 2.2-times higher amount than that in cisplatin-sensitive KF28 cells, resulting in conversion of KFr13 cells into cisplatin-sensitive cells due to an increase in cellular GM3. Exogenous GD1a also converted KFr13 cells into more responsive cells as to cisplatin, suggesting that gangliosides are involved in the cisplatin-sensitivity. Similarly, preincubation of Px2 and C13 cells with D-PDMP and GM3 effectively converted them into more responsive cells as to paclitaxel and cisplatin, respectively.

Discussion

Platinum and taxane are used as key drugs in the standard regimens for chemotherapy for ovarian cancer. Although the serous type of ovarian carcinomas is generally sensitive to these anticancer drugs in comparison to the mucinous and clear cell types, resistance to these drugs, particularly on repeated administration, remains a major obstacle for chemotherapy. More than 50% of patients originally responsive to paclitaxel and carboplatin have been reported to have recurrences within 5 years and to develop chemoresistance to these drugs (*23*). In accord with the clinical properties of the serous type of ovarian

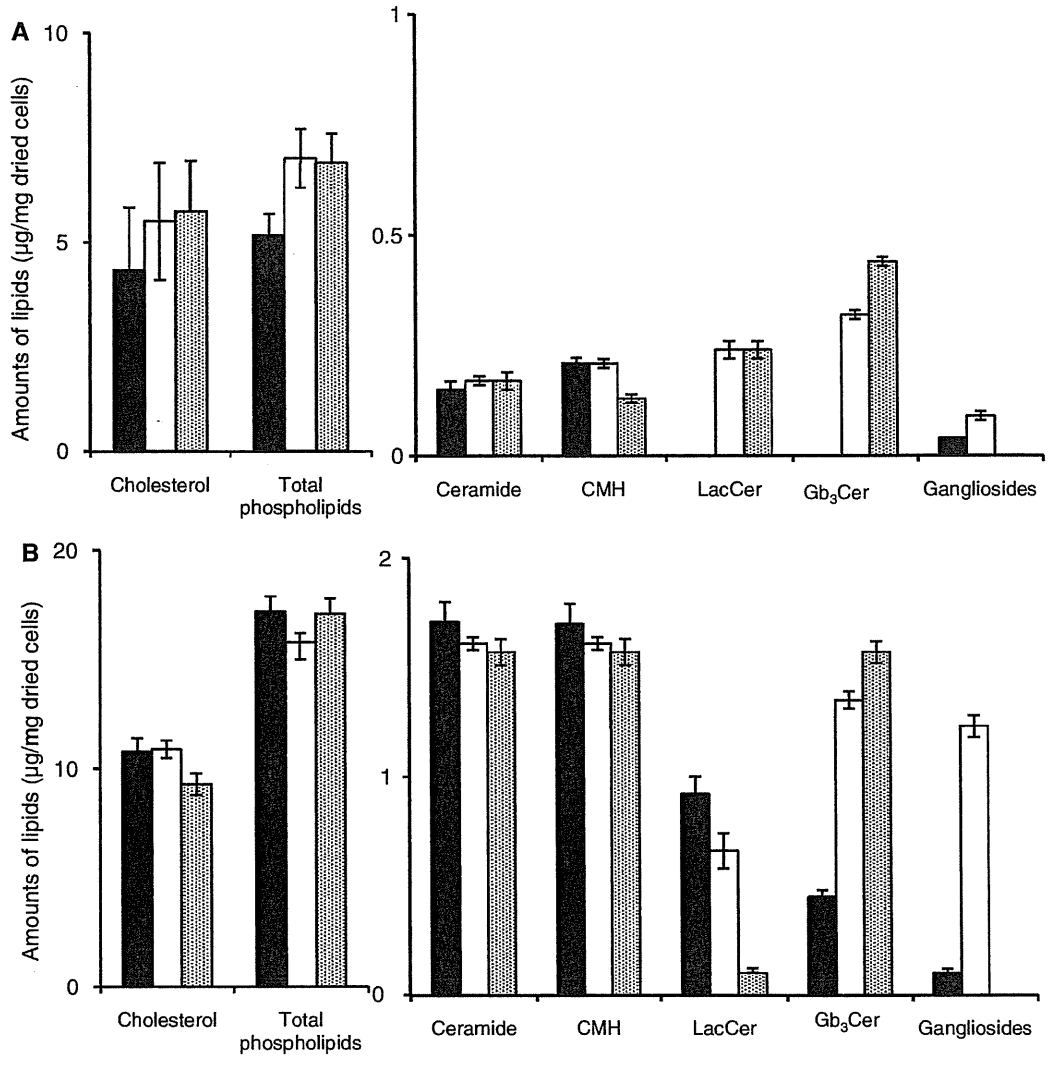

Fig. 2 Comparison of the lipid compositions of ovarian carcinoma-derived KF28 (A) and 2008 (B) cells, and their anticancer drug-resistant forms. Closed columns, original cells; open columns, paclitaxel-resistant cells; and dotted columns, cisplatin-resistant cells.

carcinomas, anticancer drug-resistant cells can be readily established from sensitive cells by continuous cultivation in media containing the respective anticancer drugs. Ovarian serous carcinoma-derived 2008 cells have been reported to exhibit stable 2- to 3-fold resistance to alkylating and platinating agents after four selections by subculture in drug-containing media, and have been frequently utilized for examination of the molecular machinery underlying anticancer drug resistance (*17*). As reported in this article, glycolipids, among the lipid constituents, of paclitaxel-resistant Px2 and cisplatin-resistant C13 cells were found to be characteristically different from those in the parent 2008 cells, and the mode of their alteration was essentially identical with that in KF28 and KF28-derived paclitaxel and cisplatin-resistant cells (*14*, *15*). Gb_3Cer was commonly increased in the paclitaxel- and cisplatin-resistant cells derived from both KF28 and 2008 ones, but its molecular species differed between KF28 and 2008-derived resistant cells, α-hydroxy and non-hydroxy fatty acid-containing ones being the major species in the former and latter cells, respectively (*14*). Because α-hydroxy fatty acids already comprise about 17% of the total fatty acids in glycolipids in the parent KF28 cells, the increase in the proportion to more than 50% of α-hydroxy fatty acids in glycolipids in both paclitaxel- and cisplatin-resistant cells was thought to be due to enhanced glycosylation into α-hydroxy fatty acid-containing ceramides as substrates. However, α-hydroxy fatty acids were not detected in the glycolipids in 2008 or 2008-derived resistant cells, even in trace amounts, probably due to a lack of α-hydroxy fatty acid synthetic potential of the parent 2008 cells.

Whereas, as to glycolipids commonly changed in both KF28- and 2008-derived cells, gangliosides were significantly increased in the paclitaxel-resistant cells, but had disappeared in the cisplatin-resistant ones. Although GM3 was the sole ganglioside in KF28 cells, and increased to twice in paclitaxel-resistant KF28TX ones, 2008 ones contained GM3, GM2 and GM1 belonging to the ganglio-series a-pathway, and

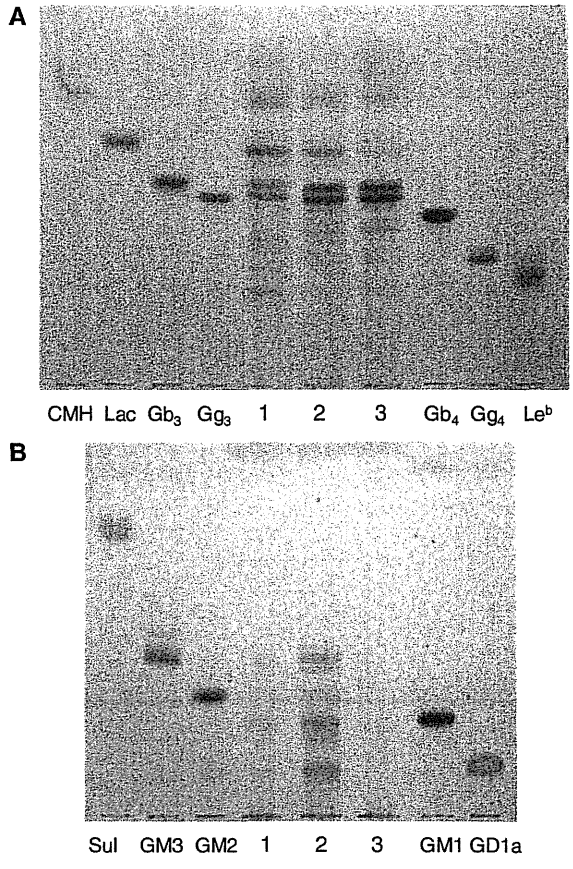

Fig. 3 TLC of neutral (A) and acidic (B) glycolipids in ovarian carcinoma-derived 2008 cells (1), paclitaxel-resistant Px2 (2) and cisplatin-resistant C13 (3) ones. The glycolipids, corresponding to 0.5 mg dry weight, were developed on TLC plates with chloroform/methanol/water (65:35:8, v/v/v) for (A) and chloroform/methanol/0.5% $CaCl_2$ in water (55:45:10, v/v/v) for (B), and were detected with orcinol sulfuric acid reagent. CMH, GalCer; Lac, LacCer; Gb_3, Gb_3Cer; Gg_3, Gg_3Cer; Gg_4, Gg_4Cer; and Sul, sulfatide.

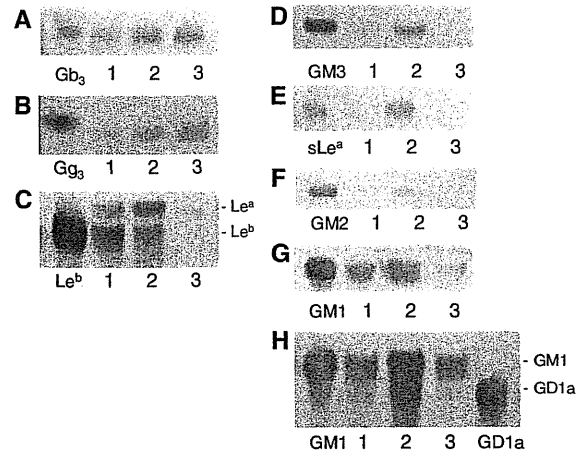

Fig. 4 TLC-immunostaining of neutral (A)–(C) and acidic (D)–(H) glycolipids in ovarian carcinoma-derived 2008 cells (1), and paclitaxel-resistant Px2 (2) and cisplatin-resistant C13 (3) ones. The glycolipids, corresponding to 0.5 mg dry weight for (A)–(G) and 0.01 mg dry weight for (H), were developed as described in Fig. 2, and then detected with carbohydrate-specific antibodies, i.e., (A) anti-Gb_3Cer; (B) anti-Gg_3Cer; (C) anti-Le^a plus Le^b; (D) anti-GM3; (E) anti-sialyl Le^a; (F) anti-GM2; and (G) anti-GM1 antibodies. For (H), the plate was firstly treated with neuraminidase and then stained with cholera toxin B subunit as described in the text.

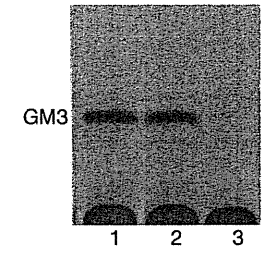

Fig. 5 Autoradiogram of products of GM3 synthase with microsomal fractions of 2008 cells and their anticancer drug-resistant forms. GM3 synthase was determined with CMP-N-acetyl [4-^{14}C]NeuAc and LacCer as substrates, and microsomal fractions of 2008 (1), Px2 (2) and C13 (3) cells, as enzyme sources, as described in the text. The products, after purification with a Sep-Pak cartridge, were developed on a TLC plate with chloroform/methanol/0.5% $CaCl_2$ in water (55:45:10, v/v/v), followed by exposure to an X-ray film.

all gangliosides together with GD1a and sialyl Le^a were increased in paclitaxel-resistant Px2 cells. Thus, paclitaxel-resistant cells were found to be active as to ganglioside synthesis, the metabolic pathways for which were possessed by the original KF28 and 2008 cells. Since gangliosides have been reported to enhance the ability of P-glycoproteins to extrude hydrophobic anticancer drugs from cells (*24*), the active synthesis of gangliosides in the paclitaxel-resistant cells might be related to enhanced expression of the MDR1 gene, which encodes P-glycoprotein, in both paclitaxel-resistant KF28TX and Px2 cells. However, our findings indicate that coexpression of the MDR1 gene and all glycolipids including gangliosides is necessary for the survival of cells in media containing paclitaxel through regulation of transporter proteins with glycolipids in membrane rafts (*16*). Glycolipids, whose amounts in paclitaxel-resistant cells were higher than those in the original cells, were LacCer, Gb_3Cer, Le^x, Le^b and GM3 for KF28TX cells and Gb_3Cer, Gg_3Cer, Gb_4Cer, Le^a, Le^b, GM3, GM2, GM1, GD1a and sialyl Le^a for Px2 cells, suggesting that all glycolipids, whose

Table III. Specific activity of GM3 synthase in ovarian carcinoma-derived KF28 and 2008 cells, and their anticancer drug-resistant forms.

Cells	Specific activity (nmol/mg protein/h)
KF28	0.18 ± 0.02
KF28TX	0.25 ± 0.05
KFr13	tr
2008	0.31 ± 0.02
Px2	0.30 ± 0.05
C13	tr

synthetic potentials were retained in the original cells, are increased in paclitaxel-resistant ones, and no characteristic structure is involved in the paclitaxel-resistance. In fact, paclitaxel-resistant cells became more sensitive on cultivation with an inhibitor of

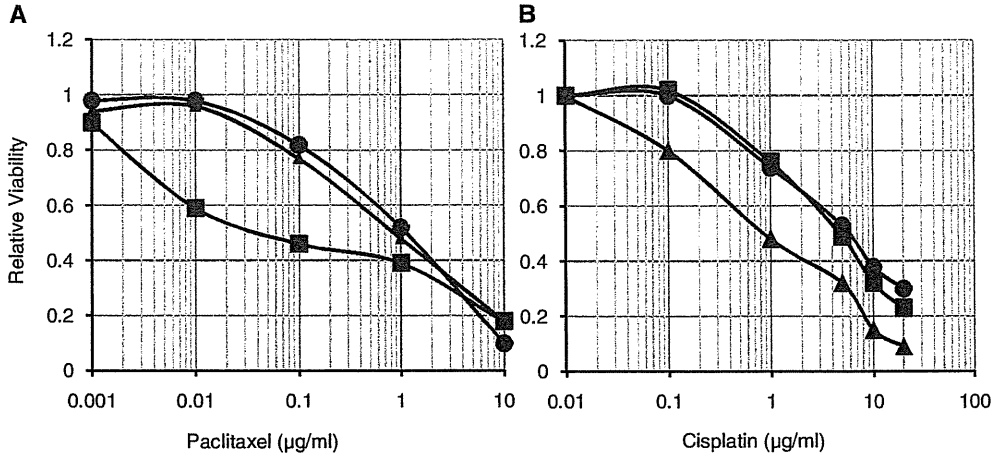

Fig. 6 Viability of KF28TX (A) and KFr13 (B) cells in media containing anticancer drugs. Paclitaxel-resistant KF28TX [•, for (A)] and cisplatin-resistant KFr13 cells [•, for (B)] were cultured in media containing 10 μM D-PDMP (■) and 10 μM GM3 (▲) for 48 h, followed by with paclitaxel (A) and cisplatin (B), and then viable cells were determined by the MTT-method as described in the text.

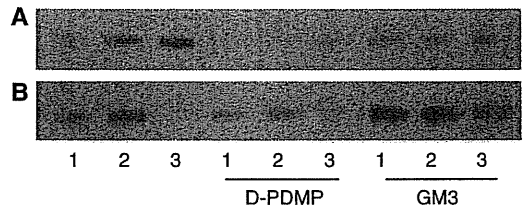

Fig. 7 TLC-immunostaining of total lipids in ovarian carcinoma-derived KF28 cells, and paclitaxel-resistant KF28TX and cisplatin-resistant KFr13 ones. KF28 (1), KF28TX (2) and KFr13 (3) cells were cultured in media containing 10 μM D-PDMP and 10 μM GM3 for 48 h and were collected by treatment with 0.05% trypsin and 0.53 mM EDTA, followed by centrifugation at 200 × g for 5 min, and the lipids were extracted from the lyophilized cells as described in the text. The lipids, corresponding to 0.5 mg dry weight, were developed with chloroform/methanol/0.5% $CaCl_2$ in water (55:45:10, v/v/v), and then detected with anti-Gb_3Cer (A) and anti-GM3 (B) antibodies as described in Fig. 4.

GlcCer synthase, D-PDMP, probably through reduced activity of transporter proteins due to retarded synthesis of glycolipids. The reason why the paclitaxel resistance of the original and cisplatin-resistant cells did not change on cultivation with D-PDMP seems to be the lowered expression of the MDR1 gene in both types compared to that in paclitaxel-resistant cells. Enhanced expression of glycolipids in hydrophobic anticancer drug-resistant cells in comparison to that in sensitive cells has also been reported in melanomas, and mammary gland and prostate carcinomas (*25–27*).

On the contrary, the gangliosides in KF28 and 2008 cells had disappeared in both KF28- and 2008-derived cisplatin-resistant cells, mainly due to a diminished activity of GM3 synthase. We suggested that increased amounts of Gb_3Cer and Gg_3Cer in cisplatin-resistant C13 and KFr13 cells were brought about by the metabolic shifts of LacCer-modifying pathway from GM3 synthase to Gb_3Cer- and Gg_3Cer-synthases, respectively. Instead of the preferential involvement of ATP-dependent transporters of hydrophobic paclitaxel in paclitaxel-resistant cells, resistance to water-soluble cisplatin has been reported to be attained through several means, i.e., reduced incorporation into cells with channels for hydrophilic drugs, enhanced extrusion through transporters, such as MRP2, and so on (*28*). Since the difference in the expression of the MRP2 gene between the original and cisplatin-resistant cells was not significant, changes in the physiochemical properties of membranes due to the altered glycolipid composition, such as lowered fluidity (*15*), might contribute to cisplatin resistance. In particular, since cultivation of cisplatin-resistant cells with exogenous GM3 resulted in a higher amount of cellular GM3 than that in cisplatin-sensitive original cells, and their conversion into a more sensitive form, the decreased amount of gangliosides might contribute to the cisplatin-resistance, probably due to the reduced incorporation of cisplatin.

On the other hand, the enhanced synthesis of glycolipids for the survival of cancer cells in the presence of anticancer drugs has been extensively studied in relation to the detoxification pathway for the removal of free ceramides that trigger apoptosis as second messengers (*11*). If the pathway for the glycosylation of ceramides derived from sphingomyelin is activated as compared with that in the parent cells, the molecular species of sphingomyelin should be reflected in those of ceramides and glycolipids in the resistant cells. As reported previously (*15*), the molecular species of sphingomyelin and ceramides in resistant cells were very similar to those in the original cells, but were distinct from those of glycolipids in the same cells, indicating that the enhanced synthesis of glycolipids in anticancer drug-resistant cells is not linked with cleavage of sphingomyelin.

On the basis of our findings, regulation of glycolipid metabolism is thought to be a useful approach for improving the effects of paclitaxel and cisplatin, respectively, and studies along these lines are now in progress in our laboratory.

Conflict of interest
None declared.

References

1. IUPAC-IUB Commission on Biochemical Nomenclature. (1977) The Nomenclature of lipids. *Eur. J. Biochem.* **79**, 11–21
2. Koprowski, H., Herlyn, M., Steplewski, Z., and Sears, H.F. (1981) Specific antigen in serum of patients with colon carcinoma. *Science* **212**, 53–55
3. Magnani, J.L., Nilsson, B., Brockhaus, M., Zopf, D., Steplewski, Z., Koprowski, H., and Ginsburg, V. (1982) A monoclonal antibody-defined antigen associated with gastrointestinal cancer is a ganglioside containing sialylated lacto-N-fucopentaose II. *J. Biol. Chem.* **257**, 14365–14369
4. Bevilacqua, M.P., Stengelin, S., Gimbrone, M.A., Jr., and Seed, B. (1989) Endothelial leukocyte adhesion molecule 1: an inducible receptor for neutrophils related to complement regulatory proteins and lectins. *Science* **243**, 1160–1165
5. Ohmori, K., Kanda, K., Mitsuoka, C., Kanamori, A., Kurata-Miura, K., Sasaki, K., Nishi, T., Tamatani, T., and Kannagi, R. (2000) P- and E-selectins recognize sialyl 6-sulfo Lewis X, the recently identified L-selectin ligand. *Biochem. Biophys. Res. Commun.* **278**, 90–96
6. Liu, F., Qi, H.L., Zhang, Y., Zhang, X.Y., and Chen, H.L. (2001) Transfection of the c-erbB2/neu gene upregulates the expression of sialyl Lewis X, alpha1,3-fucosyltransferase VII, and metastatic potential in a human hepatocarcinoma cell line. *Eur. J. Biochem.* **268**, 3501–3512
7. Aubert, M., Panicot, L., Crotte, C., Gibier, P., Lombardo, D., Sadoulet, M.O., and Mas, E. (2000) Restoration of alpha(1,2) fucosyltransferase activity decreases adhesive and metastatic properties of human pancreatic cancer cells. *Cancer Res.* **60**, 1449–1456
8. Hannun, Y.A. and Obeid, L.M. (2002) The Ceramide-centric universe of lipid-mediated cell regulation: stress encounters of the lipid kind. *J. Biol. Chem.* **277**, 25847–25850
9. Paris, F., Fuks, Z., Kang, A., Capodieci, P., Juan, G., Ehleiter, D., Haimovitz-Friedman, A., Cordon-Cardo, C., and Kolesnick, R. (2001) Endothelial apoptosis as the primary lesion initiating intestinal radiation damage in mice. *Science* **293**, 293–297
10. Sietsma, H., Veldman, R.J., and Kok, J.W. (2001) The involvement of sphingolipids in multidrug resistance. *J. Memb. Biol.* **181**, 153–162
11. Gouaze-Andersson, V. and Cabot, M.C. (2006) Glycosphingolipids and drug resistance. *Biochim. Biophys. Acta* **1758**, 2096–2103
12. Norris-Cervetto, E., Callaghan, R., Platt, F.M., Dwek, R.A., and Butters, T.D. (2004) Inhibition of glucosylceramide synthase does not reverse drug resistance in cancer cells. *J. Biol. Chem.* **279**, 40412–40418
13. Itoh, M., Kitano, T., Watanabe, M., Kondo, T., Yabu, T., Taguchi, Y., Iwai, K., Tashima, M., Uchiyama, T., and Okazaki, T. (2003) Possible role of ceramide as an indicator of chemoresistance: decrease of the ceramide content via activation of glucosylceramide synthase and sphingomyelin synthase in chemoresistant leukemia. *Clin. Cancer Res.* **9**, 415–423
14. Kiguchi, K., Iwamori, Y., Suzuki, N., Kobayashi, Y., Ishizuka, B., Ishiwata, I., Kita, T., Kikuchi, Y., and Iwamori, M. (2006) Characteristic expression of globotriaosyl ceramide in human ovarian carcinoma-derived cells with anticancer drug resistance. *Cancer Sci.* **97**, 1321–1326
15. Iwamori, M., Iwamori, Y., Kubushiro, K., Ishiwata, I., and Kiguchi, K. (2007) Characteristic expression of Lewis-antigenic glycolipids in human ovarian carcinoma-derived cells with anticancer drug-resistance. *J. Biochem.* **141**, 309–317
16. Füllekrug, J. and Simons, K. (2004) Lipid rafts and apical membrane traffic. *Ann. N. Y. Acad. Sci.* **1014**, 164–169
17. Andrews, P.A., Murphy, M.P., and Howell, S.B. (1985) Differential potentiation of alkylating and platinating agent cytotoxicity in human ovarian carcinoma cells by glutathione depletion. *Cancer Res.* **45**, 6250–6253
18. Okamoto, A., Nikaido, T., Ochiai, K., Takakura, S., Saito, M., Aoki, Y., Ishii, N., Yanaihara, N., Yamada, K., Takikawa, O., Kawaguchi, R., Isonishi, S., Tanaka, T., and Urashima, M. (2005) Indoleamine 2,3-dioxygenase serves as a marker of poor prognosis in gene expression profiles of serous ovarian cancer cells. *Clin. Cancer Res.* **11**, 6030–6039
19. Kobayashi, Y., Seino, K., Hosonuma, S., Ohara, T., Itamochi, H., Isonishi, S., Kita, T., Wada, H., Kojo, S., and Kiguchi, K. (2011) Side population is increased in paclitaxel-resistant ovarian cancer cell lines regardless of resistance to cisplatin. *Gynecol. Oncol.* **121**, 390–394
20. Bradford, M.M. (1976) A rapid and sensitive method for the quantitation of microgram quantities of protein utilizing the principle of protein-dye binding. *Anal. Biochem.* **72**, 248–254
21. Karlsson, K.A and Mårtensson, E. (1968) Studies on sphingosines. XIV. On the phytosphingosine content of the major human kidney glycolipids. *Biochim. Biophys. Acta* **152**, 230–233
22. Arita, M., Iwamori, M., Higuchi, T., and Nagai, Y. (1983) 1,1,3,3-Tetramethylurea and triethanolamine as a new useful matrix for fast atom bombardment mass spectrometry of gangliosides and neutral glycosphingolipids. *J. Biochem.* **93**, 319–322
23. McGuire, W.P., Hoskins, W.J., Brady, M.F., Kucera, P.R., Partridge, E.E., Look, K.Y., Clarke-Pearson, D.L., and Davidson, M. (1996) Cyclophosphamide and cisplatin compared with paclitaxel and cisplatin in patients with stage III and stage IV ovarian cancer. *N. Engl. J. Med.* **334**, 1–6
24. Plo, I., Lehne, G., Beckstrøm, K.J., Maestre, N., Bettaïeb, A., Laurent, G., and Lautier, D. (2002) Influence of ceramide metabolism on P-glycoprotein function in immature acute myeloid leukemia KG1a cells. *Mol. Pharmacol.* **62**, 304–312
25. Thomas, C.P., Buronfosse, A., Combaret, V., Pedron, S., Fertil, B., and Portoukalian, J. (1996) Gangliosides protect human melanoma cells from ionizing radiation-induced clonogenic cell death. *Glycoconj. J.* **13**, 377–384
26. Ravindranath, M.H., Muthugounder, S., Presser, N., Selvan, S.R., Portoukalian, J., Brosman, S., and Morton, D.L. (2004) Gangliosides of organ-confined versus metastatic androgen-receptor-negative prostate cancer. *Biochem. Biophys. Res. Commun.* **324**, 154–165
27. Prinetti, A., Basso, L., Appierto, V., Villani, M.G., Valsecchi, M., Loberto, N., Prioni, S., Chigorno, V., Cavadini, E., Formelli, F., and Sonnino, S. (2003) Altered sphingolipid metabolism in N-(4-hydroxyphenyl)-retinamide-resistant A2780 human ovarian carcinoma cells. *J. Biol. Chem.* **278**, 5574–5583
28. Huang, Y. and Sadée, W. (2006) Membrane transporters and channels in chemoresistance and -sensitivity of tumor cells. *Cancer Lett.* **239**, 168–182

Cancer Science
The official journal of the Japanese Cancer Association

Proteomic characterization of ovarian cancers identifying annexin-A4, phosphoserine aminotransferase, cellular retinoic acid-binding protein 2, and serpin B5 as histology-specific biomarkers

Atsuhiko Toyama,[1] Atsushi Suzuki,[2] Takashi Shimada,[1] Chikage Aoki,[1] Yutaka Aoki,[1] Yukari Umino,[1] Yusuke Nakamura,[3] Daisuke Aoki[2] and Taka-Aki Sato[1,4]

[1]Life Science Research Center, Shimadzu Corporation, Tokyo; [2]Department of Obstetrics and Gynecology, School of Medicine, Keio University, Tokyo; [3]Human Genome Center, Institute of Medical Sciences, University of Tokyo, Tokyo, Japan

(Received October 24, 2011/Revised December 28, 2012/Accepted January 4, 2012/Accepted manuscript online February 9, 2012/Article first published online February 20, 2012)

Numerous studies have suggested that the different histological subtypes of ovarian carcinoma (i.e. clear cell, endometrioid, mucinous, and serous) have distinct clinical histories and characteristics; however, most studies that have aimed to determine biomarker have not performed comprehensive analyses based on subtype specificity. In the present study, we performed two-dimensional gel electrophoresis-based differential proteomic analysis of the different histological subtypes of ovarian carcinoma using tissue specimens from 39 patients. Seventy-seven protein spots (55 unique proteins) were found to be up- or downregulated in a subtype-specific manner. The most significant difference was observed for: (i) annexin-A4 (ANXA4) and phosphoserine aminotransferase (PSAT1), which are expressed strongly in clear cell carcinoma; (ii) cellular retinoic acid-binding protein 2 (CRABP2), which is expressed specifically in serous carcinoma; and (iii) serpin B5 (SPB5), which is upregulated in mucinous carcinoma. Validation of these candidates by western blotting using a 34 additional test sample set resulted in an expression pattern that was consistent with the screening and revealed that differential expression was independent of cancer stage or tumor grade within each subtype. Thus, the present study reinforces the notion that ovarian cancer subtypes can be clearly delineated on a molecular basis into four histopathological groups, and we propose that ANXA4, PSAT1, CRABP2, and SPB5 are candidate subtype-specific biomarkers that can help define the basis of tumor histology at a molecular level. (*Cancer Sci* 2012; 103: 747–755)

Epithelial ovarian carcinomas (EOC) are grouped histopathologically into serous, endometrioid, mucinous, and clear cell carcinomas. These subtypes have been suggested to differ in their oncogenic mechanisms,[1] precursor lesions,[2,3] risk factors,[4] and molecular signatures as determined by mRNA expression profiling.[5] Clinically, EOC subtypes respond differently to chemotherapy. For example, clear cell carcinoma is relatively resistant to chemotherapy, with approximately 30% of cases responding to combination therapy with carboplatin and paclitaxel (TC regimen),[6] resulting in a relatively poor prognosis and high recurrence rate.[7] Clear cell carcinoma is also unique in that its incidence is markedly higher in Japan than in Western countries and is rising.[8] Although current clinical practices regard EOC as a single disease entity and treatment regimens are not subtype specific, the evidence from the literature suggests that EOC is a multifaceted disease with subtypes that have distinct clinical features. However, the recent NCI State of Science meeting proposed that separate clinical trials for mucinous and clear cell EOC subtypes be undertaken.[9] Moreover, a recent study argued that biomarkers that take subtype specificity into account could convey more information by demonstrating that the association between prognosis and Wilms' tumor-1 expression was unique to the serous subtype.[10]

The aim of the present study was to discover better candidate biomarkers for EOC that were associated with the histopathological classification by identifying proteins that were correlated with specific subtypes. Using clinical tissue specimens we undertook the expression profiling of clear cell, endometrioid, mucinous and serous carcinoma using two-dimensional gel electrophoresis (2-DE)-based differential proteomic analysis. Although extensive profiling studies have been performed using mRNA microarray,[11–15] only a handful of studies have undertaken proteomic analysis of EOC[16–19] and many of the studies have experimental shortcomings, such as insufficient sample size, analysis of only a single subtype, or analyses based on cell lines.

To overcome these issues, we used 39 fresh frozen ovarian cancer specimens for differential analysis and 34 additional specimens for validation of a number of promising targets. This is the first report to describe the comprehensive proteomic expression profile of EOC subtypes.

Materials and Methods

Ovarian cancer specimens. Ovarian cancer samples were collected from patients who had provided informed consent by Keio University Hospital, with the approval of the Ethics Committee of Keio University (Approval No. 15-96-6). The characteristics of the samples used are summarized in Table 1, with details provided in Table S1. Resected tumor samples were snap frozen in liquid nitrogen and stored at −150°C until protein extraction. Cancer staging in the present study adhered to the International Federation of Gynecology and Obstetrics (FIGO) criteria.[20]

The present study was approved by the Keio University Institutional Review Board.

Reagents. DeStreak Reagent, IPG buffer, Immobiline DryStrip gel, HRP-conjugated anti-rabbit IgG, the ECL detection

[4]To whom correspondence should be addressed.
E-mail: takaaki@shimadzu.co.jp

doi: 10.1111/j.1349-7006.2012.02224.x

Table 1. Summary of the ovarian cancer specimens used in the present study

	Epithelial ovarian carcinoma subtype			
	Clear cell	Endometrioid	Mucinous	Serous
n	13	10	6	10
FIGO stage				
Stage I	10	4	6	0
Stage II	0	2	0	5
Stage III	3	4	0	5
Tumor grade				
Grade 1	N/A	5	6	0
Grade 2	N/A	2	0	6
Grade 3	N/A	3	0	4
Mean age at diagnosis (years)	55	48	54	54

FIGO, the International Federation of Gynecology and Obstetrics.

kit and chemiluminescence films were purchased from GE Healthcare (Buckinghamshire, UK). The HRP-conjugated anti-β-actin antibody (Sp2/0-Ag14) was obtained from Abcam (Cambridge, UK). Sequence grade modified trypsin was from Promega (Madison, WI, USA). ZipTip μC18 was from Millipore (Madison, WI, USA). The MALDI matrix, α-cyano-4-hydroxycinnamic acid, was purchased from Shimadzu-GLC (Tokyo, Japan).

Two-dimensional gel electrophoresis. Frozen tissue blocks were first pulverized in liquid nitrogen, transferred to screw-cap microtubes, and homogenized in buffer composed of 50 mM HEPES–NaOH, pH 7.5, 100 mM NaCl, 2% CHAPS, and 1% Triton X-100. Lysis was performed by using a ball mill homogenizer operated at 4000/min for 1 min with zirconium beads (1 mm diameter; Tomy Seiko, Tokyo, Japan). After centrifugation at 20 000*g* for 15 min, the supernatant was collected for 2-DE analysis. For 2-DE, tissue extracts containing 300 μg total protein were desalted by 15% trichloroacetic acid precipitation followed by cold ethanol/ether washing and then redissolved in buffer containing 6 M urea, 2 M thiourea, 2% CHAPS, 1% Triton X-100, 0.5% DeStreak Reagent and 0.5% IPG buffer. Isoelectric focusing was performed using a 13-cm Immobiline DryStrip, pH 3–10, non-linear gel, whereas a 10–18% linear gradient polyacrylamide gel was used for second-dimension SDS-PAGE. Protein spots were visualized by 0.1% Coomassie brilliant blue G-250 stain and gel images were acquired using a GS-800 Imaging Densitometer (Bio-Rad Laboratories, Hercules, CA, USA).

Analysis of 2-DE data. The 2-DE gel images were analyzed using Progenesis PG200 software ver. 2006.2160.3 (Nonlinear Dynamics, Newcastle, UK) to compute spot detection and density calculations. Detected spots were matched across all gels while manually flagging poor-quality spots. The background level was computed according to the modal density in the 50-pixel margin surrounding each spot and subtracted accordingly. Spot volume was normalized by dividing each spot volume by the sum of all matched spots (excluding large spots derived from blood, such as albumin), followed by further division by the β-actin spot on the same gel, thereby collectively correcting for the variation in total loading amount and blood proteins. As a consistency criterion, all spots observed at frequency of <50% in all histological subtypes were excluded from further analyses. Absent spots were given an arbitrary expression value of either the smallest value among the matched spot set or one-third of the mean, whichever gave the smaller value. In all, 323 spots that fulfilled the consistency criterion were identified by mass spectrometry (Table S2). Subtype-specific expression was tested by the Mann–Whitney *U*-test. For each spot, *P*-values were calculated with respect to each subtype testing the null hypotheses $\text{median}_{\text{subtype}} = \text{median}_{\text{all}}$. The Mann–Whitney *U*-test, Spearman's correlation (rho) test, and principal component analysis were performed using SPSS ver. 15.0J (IBM, Tokyo, Japan). Computed principal components were subsequently transformed by varimax rotation and the first two principal components were used for scatter plot display. Gene ontology (GO) annotation for the listed proteins was collected from QuickGO (http://www.ebi.ac.uk/QuickGO/, accessed 20 May 2011) using the GO slim algorithm.[21]

Protein identification. Protein spots were excised to gel pieces that were 1.5 mm in diameter and transferred to a 96-well microtiter plate. In-gel trypsin digestion was performed as described by Shevchenko *et al.*[22] using 50 ng sequencing grade modified trypsin per gel piece. Extracted peptides were desalted by ZipTip μC18 and eluted directly onto a matrix-assisted laser desorption ionization (MALDI) target plate. The MALDI matrix, α-cyano-4-hydroxycinnamic acid, was prepared at a concentration of 3 mg/mL in aqueous 50% acetonitrile and 10 mM ammonium dihydrogen phosphate, and 0.5 μL was applied to each well. After drying, peptide mass fingerprints were acquired using the AXIMA-CFRplus MALDI time-of-flight mass spectrometry (MALDI-TOF MS) instrument (Shimadzu/Kratos, Kyoto, Japan) for *m/z* 700–3500. Proteins were identified by MASCOT Server ver. 2.3.02 (Matrix Sciences, London, UK), searching against 20 239 human sequences of UniProt (http://www.uniprot.org/, accessed 1 Jun 2011, database release 2011_05). The search parameters were as follows: enzyme, trypsin; allow up to one missed cleavage; carbamidomethyl (cysteine) fixed modification; oxidation (methionine) and acetylation (protein N-terminus) variable modifications; peptide tolerance 0.15 Da. Protein spots were regarded as identified only when confirmed by at least two independent identification results acquired from the same position of different 2-DE gels of ovarian cancer samples. For acid ceramidase only, protein identification was assisted by an MS/MS ion search by AXIMA-QIT (Shimadzu/Kratos) using a fresh preparation.

Western blotting. Target proteins annexin A4 (ANXA4), cellular retinoic acid-binding protein 2 (CRABP2), serpin B5 (SPB5), and phosphoserine aminotransferase (PSAT1) were quantified by western blotting using the same tissue lysates as used for biomarker screening plus an independent sample set. Total protein (5 μg) was separated by tricine-buffered SDS-PAGE and blotted on a PVDF membrane. Polyclonal antibodies were produced by immunization of rabbits with human full-length recombinant ANXA4, CRABP2, SPB5, and PSAT1, and used at a dilution of 1:2000 using 5% skim milk as a blocking agent. The HRP-conjugated secondary antibody was used at a dilution of 1:5000 in 2% BSA. Reactivity was visualized on chemiluminescence films using an ECL detection kit (GE Healthcare). Directly after detection, the membranes were washed twice in 100 mM glycine–HCl pH 2.5 buffer, blocked in 5% skim milk and reprobed with HRP-conjugated anti-β-actin as a loading control.

Immunohistochemistry. Formalin-fixed, paraffin-embedded tissues from EOC patients were sectioned at 4 μm. All slides were deparaffinized in xylene and rehydrated by stepwise immersion (for 2 min each) in 100%, 100%, 90%, 80%, and finally 70% ethanol. Residual peroxidase activity was quenched in 0.3% hydrogen peroxide in methanol for 30 min. Immunohistochemical staining was performed using the VECTASTAIN Elite ABC kit and ImmPACT DAB solution (Vector Laboratories, Burlingame, CA, USA) according to the manufacturer's instructions. The primary antibodies were anti-ANXA4 antibody (clone D-2; 1:200 dilution; Santa Cruz), anti-SPB5 antibody (clone EAW24; 1:20 dilution; Thermo Fisher Scientific, Waltham, MA, USA), anti-CRABP2 antibody (clone TA52; 1:

doi: 10.1111/j.1349-7006.2012.02224.x

2000 dilution; Chemicon, Temecula, CA, USA), and anti-PSAT1 polyclonal antibody (product code 10501-1-AP; 1:100 dilution; Proteintech, Chicago, IL, USA). For antigen retrieval for SPB5, CRABP2 and PSAT1 staining, slides were boiled in 10 mM citrate buffer (pH 5.0) at 110°C for 1 min in an autoclave and anti-SPB5 antibody was diluted in Can Get Signal Immunostain Solution B (Toyobo, Osaka, Japan). Stained sections were lightly counterstained with hematoxylin and then examined under a light microscope (DM6000B; Leica Microsystems, Wetzlar, Germany).

Results

Proteomic profiling by 2-DE. Surgically dissected tissue blocks of 39 ovarian cancer patients (Table 1) were prepared and the total protein content in each was differentially analyzed by 2-DE to compare clinically important histological subtypes: clear cell, endometrioid, mucinous, and serous adenocarcinoma. The screening process is summarized in Figure 1. Representative 2-DE images of each subtype are shown in Figure 2(a), detecting a total of 800–900 protein spots. As described previously,[23] each spot volume was normalized against the β-actin spot. After spot matching and the application of consistency criteria, 323 spots were selected for further analysis and were identified by MALDI-TOF MS, giving 217 unique protein identities. The expression levels of the identified spots in each subtype were compared against all other subtypes combined by the Mann–Whitney *U*-test to elucidate subtype-specific features. Table 2 lists those proteins that were significantly up- or downregulated ($P < 0.0125$, considering Bonferroni's correction). In total, 77 spots (55 proteins) were identified as potential subtype-specific biomarker candidates. According to the cellular_component of the GO annotation, the screened proteins were mostly cytoplasmic and demonstrated that the influence of blood on our tissue proteome analysis was minimal. As indicated in parentheses following the protein names in Table 2, redundancy in protein identification was frequently observed owing to multiple conformations of the same protein separating into individual spots. Differential expression observed in only one of the multiple spots was possibly indicative of a subtype-specific change in protein modification, such as phosphorylation, acetylation, glycosylation, or site-specific protease cleavage. For example, Spots 1

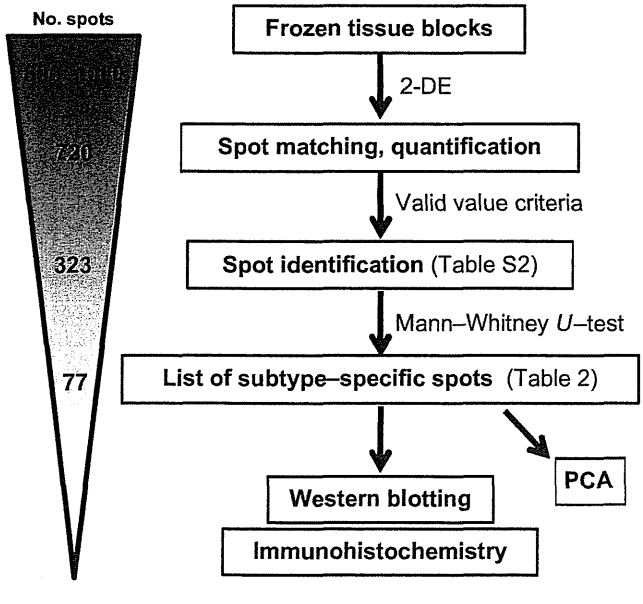

Fig. 1. Overall workflow of the screening performed in the present study. 2-DE, two-dimensional gel electrophoresis; PCA, principal component analysis.

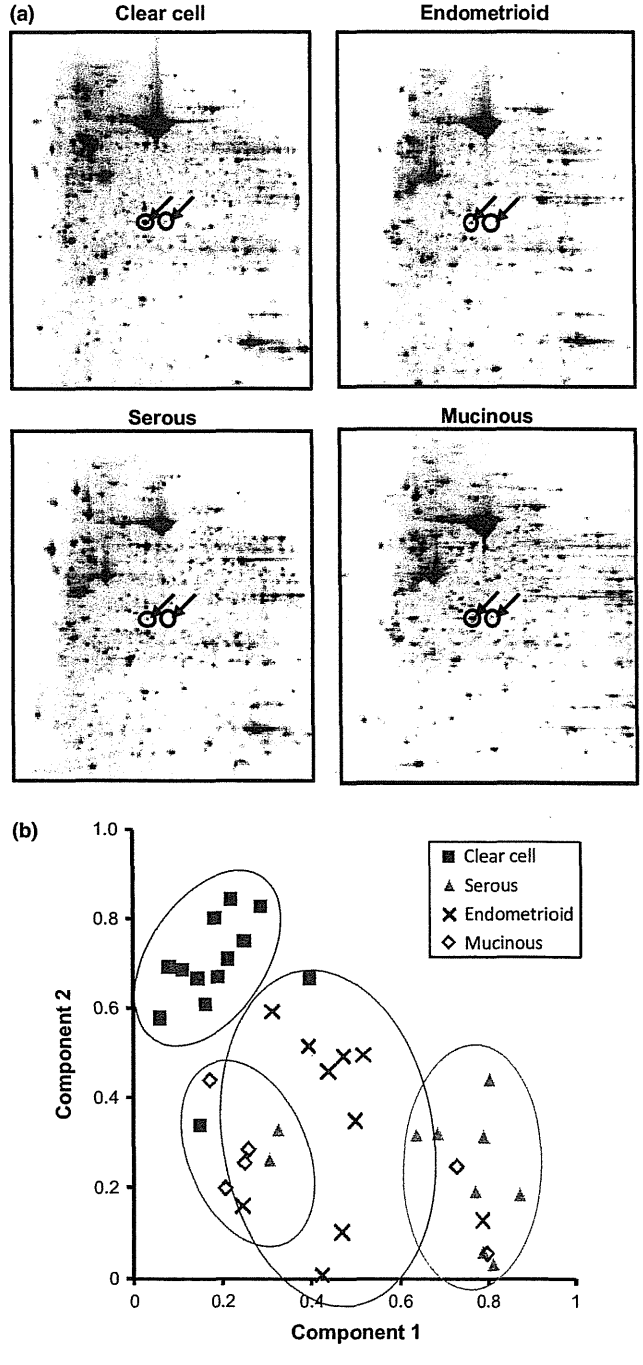

Fig. 2. Seventy-seven differentially expressed spots were identified by two-dimensional (2D) gel electrophoresis analysis of epithelial ovarian carcinoma subtypes. (a) Representative 2D gel images of clear cell, endometrioid, serous, and mucinous tumor lysates, separated over a pH 3–10NL gel in the first dimension and a 10–18% gradient gel in the second dimension. Arrows indicate the position of annexin-A4 spots. (b) Scatter plot of the first two components computed using the expression values of 77 subtype-specific spots with $P < 0.0125$, showing separation of clear cell carcinoma from the other subtypes. Individual tumors are annotated with histological subtype as indicated.